COO-2245-42TR

DEPARTMENTS OF NUCLEAR AND MECHANICAL ENGINEERING
MASSACHUSETTS INSTITUTE OF TECHNOLOGY
Cambridge, Massachusetts 02139

July, 1977

PRESSURE DROP MEASUREMENTS IN LMFBR WIRE WRAPPED BLANKET ASSEMBLIES

by

C. Chiu
J. Hawley
W.M. Rohsenow
N.E. Todreas

ERDA Research and Development
Contract E(11-1)-2245
U.S. Energy Research and Development Administration

DISCLAIMER

Reports and Papers Published under
MIT Coolant Mixing in LMFBR Rod Bundles Project

A. Quarterly Progress Reports (Available from National Technical Information Service, U.S. Department of Commerce, Springfield, VA 22151)

COO-2245-1	Period June 1, 1972 - November 30, 1972
COO-2245-2	Period December 1, 1972 - February 28, 1973
COO-2245-3	Period March 1, 1973 - May 31, 1973
COO-2245-6	Period June 1, 1973 - August 31, 1973
COO-2245-7	Period September 1, 1973 - November 30, 1973
COO-2245-8	Period December 1, 1973 - February 28, 1974
COO-2245-10	Period March 1, 1974 - May 31, 1974
COO-2245-13	Period June 1, 1974 - August 31, 1974
COO-2245-14	Period September 1, 1974 - November 31, 1974
COO-2245-15	Period December 1, 1974 - February 28, 1975
COO-2245-23	Period March 1, 1975 - May 31, 1975
COO-2245-25	Period June 1, 1975 - August 31, 1975
COO-2245-26	Period September 1, 1975 - November 30, 1975
COO-2245-28	Period December 1, 1975 - February 29, 1976
COO-2245-30	Period March 1, 1976 - May 31, 1976
COO-2245-31	Period June 1, 1976 - August 31, 1976
COO-2245-34	Period September 1, 1976 - November 30, 1976
COO-2245-38	Period December 1, 1976 - February 28, 1977
COO-2245-50	Period March 1, 1977 - May 31, 1977
COO-2245-53	Period June 1, 1977 - August 31, 1977

Reports Issued Under This Contract

B. Topical Reports (Available from National Technical Information Service, U.S. Department of Commerce, Springfield, VA 22151)

E. Khan and N. Todreas, "A Review of Recent Analytical and Experimental Studies Applicable to LMFBR Fuel and Blanket Assembly Design," COO-2245-4TR, MIT, Sept. 1973.

E. Khan, W. Rohsenow, A. Sonin and N. Todreas, "A Simplified Approach for Predicting Temperature Distribution in Wire Wrapped Assemblies," COO-2245-5TR, MIT, Sept. 1973.

T. Eaton and N. Todreas, "Instrumentation Methods for Interchannel Coolant Mixing Studies in Wire-Wrap Spaced Nuclear Fuel Assemblies," COO-2245-9TR, MIT, June 1974.

Y.B. Chen, K. Ip, N.E. Todreas, "Velocity Measurements in Edge Subchannels of Wire Wrapped LMFBR Fuel Assemblies," COO-2245-11TR, MIT, September 1974.

E. Khan, N. Todreas, W. Rohsenow, A.A. Sonin, "Analysis of Mixing Data Relevant to Wire-Wrapped Fuel Assembly Thermal-Hydraulic Design," COO-2245-12TR, MIT, September 1974.

E. Khan, W. Rohsenow, A. Sonin, N. Todreas, "A Porous Body Model for Predicting Temperature Distributions in Wire Wrapped Fuel and Blanket Assemblies of a LMFBR," COO-2245-16TR, MIT, March 1975.

E. Khan, W.M. Rohsenow, A. Sonin, N. Todreas, "Input Parameters to the ENERGY Code (To be used with the ENERGY Code Manual) COO-2245-17TR, MIT, May 1975.

E. Khan, W. Rohsenow, A. Sonin, N. Todreas, "Manual for ENERGY Codes I, II, III," COO-2245-18TR, MIT, May 1975

E. Khan, W. Rohsenow, A. Sonin, N. Todreas, "Manual for ENERGY Codes I, II, III Computer Programs," COO-2245-18TR Revision 1, MIT, July 1976.

P. Carajilescov and N. Todreas, "Experimental and Analytical Study of Axial Turbulent Flows in an Interior Subchannel of a Bare Rod Bundle," COO-2245-19TR, MIT.

B. Chen and N. Todreas, "Prediction of Coolant Temperature Field in a Breeder Reactor Including Interassembly Heat Transfer," COO-2245-20TR, MIT, May 1975.

B. Chen and N. Todreas, "Prediction of Coolant Temperature Field in a Breeder Reactor Inlcuding Interassembly Heat Transfer," COO-2245-20TR Revision 1, MIT, December 1976.

F. Carre and N. Todreas, "Development of Input Data to ENERGY Code for Analysis of Reactor Fuel Bundles," COO-2245-21TR, MIT, May 1975.

Reports Issued Under This Contract

B. Topical Reports, Continued

H. Ninokata and N.E. Todreas, "Turbulent Momentum Exchange Coefficients for Reactor Fuel Bundle Analysis," COO-2245-22TR, MIT, June 1975.

R. Anoba and N. Todreas, "Coolant Mixing in LMFBR Rod Bundles and Outlet Plenum Mixing Transients," COO-2245-24TR, August 1975.

B. Bosy, "Fabrication Details for Wire Wrapped Fuel Assembly Components," COO-2245-27TR, MIT, November 1975.

Ralph G. Bennett and Michael W. Golay, "Interferometric Investigation of Turbulently Fluctuating Temperature in an LMFBR Outlet Plenum Geometry," COO-2245-29TR, MIT, June 1976.

N.E. Todreas, "Analysis Methods for LMFBR Wire Wrapped Bundles," COO-2245-32TR, MIT, November 1976.

K.L. Basehore and N.E. Todreas, "Development of Stability Criteria and an Interassembly Conduction Model for the Thermal-Hydraulics Code SUPERENERGY," COO-2245-33TR, MIT December 1976.

Robert Masterson and Neil E. Todreas, "Analysis of the Feasibility of Implementing an Implicit Temporal Differencing Scheme in the SUPERENERGY Code," COO-2245-35TR, MIT, February 1977.

S. Glazer, C. Chiu and N. Todreas, "Collection and Evaluation of Salt Mixing Data with the Real Time Data Acquisition System," COO-2245-36TR, MIT, April 1977.

B. Mikic, E.U. Khan and N.E. Todreas "An Approximate Method for Predicting Temperature Distribution in Wire Wrapped Fuel Assemblies of a LMFBR," COO-2245-37TR, MIT, April 1977.

C. Chiu and N. Todreas, "Development of a Technique for Subchannel Flow Rate Measurements in LMFBR Wire Wrapped Assemblies," COO-2245-39TR, July 1977

C. Chiu and N. Todreas, "WARD Blanket Assembly Pre-Test Predictions by SUPERENERGY," COO-2245-40TR, July 1977

C. Chiu and N. Todreas, "Flow Split for a LMFBR 4" Wire Wrapped Blanket Assembly," COO-2245-41TR, July 1977

C. Chiu and N. Todreas, "Static Pressure and Pressure Drop for a LMFBR 4" Wire Wrapped Blanket Assembly," COO-2245-42TR, July 1977

Reports Issued Under This Contract

B. Topical Reports, Continued

C. Chiu and N. Todreas, "Mixing Experiments for a LMFBR 4" Wire Wrapped Blanket Assembly," COO-2245-43TR, July 1977

Yi Bin Chen and Michael W. Golay, "Coolant Mixing in the LMFBR Outlet Plenum," COO-2245-44TR, June 1977.

J. Kelly and N. Todreas, "Turbulent Interchange in Triangular Array Bare Rod Bundles," COO-2245-45TR, July 1977

K.L. Basehore and N.E. Todreas, "Assessment of the Need to Incorporate a Variable Swirl Flow Model into the ENERGY Code," COO-2245-46TR, July 1977.

K.L. Basehore and N. Todreas, "Analysis of the Thermal-Hydraulic Behavior in the CRBR Secondary Control Assembly, Including Interassembly Heat Transfer Effects," COO-2245-47TR, July 1977.

J.G. Bartzis and N.E. Todreas, "Hydrodynamic Behavior of a Bare Rod Bundle," COO-2245-48TR, June 1977.

M.R. Fakori-Monazah and N.E. Todreas, "Measurement and Analysis of Flow Wall Shear Stress in an Interior Subchannel of Triangular Array Rods," COO-2245-49TR, August 1977.

A.S. Hanson and N.E. Todreas, "Fluid Mixing Studies in an Hexagonal 61-Pin, Wire-Wrapped Rod Bundle," COO-2245-51TR, August 1977.

S. Glazer, N. Todreas, W. Rohsenow, and A. Sonin, "TRANSENERGY S,M - Computer Codes for Coolant Temperature Prediction in LMFBR Cores During Transient Events," COO-2245-52TR, January 1977.

C. Chiu, W.M. Rohsenow and N.E. Todreas, "Mixing Experiments in an Alternating Wire Wrapped Assembly," COO-2245-54TR, MIT, December 1977.

C. Chiu, W.M. Rohsenow and N. E. Todreas, "Sweeping Flow Mixing Model for Wire Wrapped LMFBR Assemblies," COO-2245-55TR, MIT, December 1977.

C. Chiu, W.M. Rohsenow and N.E. Todreas, "Lumped Subchannel Flow Model for LMFBR Wire Wrapped Assemblies," COO-2245-56TR MIT, December 1977.

Reports Issued under this Contract

C. Papers and Summaries

Yi Bin Chen, Ka-Lam Ip, Neil E. Todreas, "Velocity Measurements in Edge Channels of Wire-Wrapped LMFBR Fuel Assemblies," American Nuclear Society Transactions Vol. 19, 1974, pp. 323-324.

P. Carajilescov, N. Todreas, "Experimental and Analytical Study of Axial Turbulent Flows in an Interior Subchannel of a Bare Rod Bundle," J. of Heat Transfer, Vol. 98, No. 2, May 1976, pp. 262-268 (Included as Appendix to Quarterly Progress Report, COO-2245-15).

E. Khan, W. Rohsenow, A. Sonin, N. Todreas, "A Porous Body Model for Predicting Temperature Distribution in Wire-Wrapped Fuel Rod Assemblies," Nuclear Engineering and Design, 35 (1975) 1-12.

E. Khan, W. Rohsenow, A. Sonin, N. Todreas, "A Porous Body Model for Predicting Temperature Distribution in Wire-Wrapped Rod Assemblies Operating in Combined Forced and Free Convection," Nuclear Engineering and Design, 35 (1975) 199-211.

Ralph G. Bennett and Michael W. Golay, "Development of an Optical Method for Measurement of Temperature Fluctuation in Turbulent Flows," American Nuclear Society Transactions, Vol. 22, 1975, p. 581.

B. Chen and N. Todreas, "Prediction of the Coolant Temperature Field in a Breeder Reactor Including Interassembly Heat Transfer," Nuclear Engineering and Design 35, (1975) 423-440 (Included as Appendix to Quarterly Progress Report, COO-2245-23).

R. Bennett and M.W. Golay, "Interferometric Investigation of Turbulently Fluctuating Temperature in an LMFBR Outlet Plenum Geometry," Accepted for the ASME Winter Annual Meeting, Dec., 1976, (Included as Appendix in Quarterly Progress Report, COO-2245-30).

B.B. Mikic, E.U. Khan, N.E. Todreas, "An Approximate Method for Predicting Temperature Distribution in Wire Wrapped Fuel Assemblies of a Liquid Metal Fast Breeder Reactor," Mech. Res. Comm., Vol. 3, 353-360 (1976).

Reports Issued Under this Contract

C. Papers and Summaries (Continued)

L. Wolf, R. Karimi, I.Y. Kim, C.N. Wong, M.K. Yeung "2-D Thermoelastic Analysis of LMFBR Fuel Rod Claddings," Paper C4/d, 4th International Conf. Structural Mechanics in Reactor Technology, San Francisco, August 1977.

M. Yeung, L. Wolf, "Effective Conduction Mixing Lengths for Subchannel Analysis of Finite Hexagonal LMFBR Bundles," ANS Meeting, New York, June 1977.

C. Chiu and N. Todreas, "Flow Split Measurements In An LMFBR Radial Blanket Assembly," ANS Meeting, New York, June 1977.

"This report was prepared as an account of Government-sponsored work. Neither the United States, or the Energy Research and Development Administration nor any person acting on behalf of the Commission

A. Makes any warranty or representation, expressed or implied, with respect to the accuracy, completeness or usefulness of the information contained in this report, or that the use of any information, apparatus method, or process disclosed in this report may not infringe privately owned rights; or

B. Assumes any liabilities with respect to the use of, or for damages resulting from the use of, any information, apparatus, method, or process disclosed in this report.

As used in the above, 'person acting on behalf of the Commission' includes any employee or contractor of the Administration or employee of such contractor, to the extent that such employee or contractor prepares, disseminates, or provides access to, any information pursuant to his employment or contract with the Administration or his employment with such contractor."

ABSTRACT

In this experiment, measurements of subchannel static pressure for an interior and edge subchannel were taken at two elevations in two wire-wrapped 61-pin bundles. One of the bundles has geometric characteristics of P/D = 1.067 and H/D = 8.0 (4 inch lead length and 0.501 inch rod diameter) and the other bundle has geometric characteristics of P/D = 1.067 and H/D = 4.0 (2 inch lead length and 0.501 inch rod diameter).

The bundle average friction factors as well as the local subchannel friction factors for both interior and edge subchannels were determined from the experimental static pressure data. The average subchannle flow rates for both edge and interior subchannels were determined in a separate experiment. Results show that two correlations suggested by Rehme and Novendstern for the bundle average friction factor cannot predict the data within the range of experimental error. The bundle average friction factors for both bundles under test were underestimated by Rehme's correlation and overestimated by Novendstern's correlation.

The results of the local subchannel friction factors indicate the effect of the wire wrap lead length is more pronounced in the interior subchannel friction factor than in the edge subchannel friction factor. As the wire wrap lead length decreases, both interior and edge subchannel friction factors increase.

ACKNOWLEDGEMENTS

The authors would like to thank Mr. Mike Corradini for his valuable suggestions and editing. Thanks are also due to Ms. Jacqueline Humbert for her tireless editing and proofreading of the final draft of this report.

The authors wish to thank Malka Grinkorn and Ginny O'Keefe for their typing.

Sponsorship of this work through the Energy Research and Development Administration is also acknowledged.

NOMENCLATURE

D	Fuel pin diameter, (ft)
D_e	Average bundle equivalent hydraulic diameter, defined as the ratio of four times the total bundle area to the total bundle wetted perimeter, (ft).
Des	Subchannel equivalent hydraulic diameter.
D_{e2}	Equivalent hydraulic diameter of edge subchannels, (ft)
D_{e1}	Equivalent hydraulic diameter of interior subchannels, (ft)
f_b	Bundle average friction factor, defined by Eq. (4-1)
f_s	Local subchannel friction factor, defined by Eq. (4-8)
f_{s2}	Local edge subchannel friction factor
f_{s1}	Local interior subchannel friction factor
H	Wire wrap lead (or pitch), (ft)
L	Bundle or subchannel length over which the pressure drop is measured, (ft)
N	Total number of subchannels in test bundles
N_1	Total number of interior subchannels in test bundles
N_2	Total number of edge subchannels in test bundles
N_3	Total number of corner subchannels in test bundles
N_R	Total number of rods in test bundles
P	Fuel rod pitch (ft)
Re	Average bundle Reynolds number characterized by the bundle average equivalent hydraulic diameter and the bundle average velocity
Re_2	Edge subchannel Reynolds number, defined by Eq. (4-12)

Re_1	Interior subchannel Reynolds number, defined by Eq. (4-9).
V_b	Bundle average velocity, (ft/hr).
V_1	Interior subchannel average velocity (over a lead length), (ft/hr).
V_s	Subchannel average velocity (over one lead length), (ft/hr).
V_2	Edge subchannel average velocity (over a lead length), (ft/hr)
x_1	Interior subchannel flow split parameter, defined as the ratio of interior subchannel velocity (averaged over a lead) to the bundle average velocity.
x_2	Edge subchannel flow split parameter, defined as the ratio of the edge subchannel velocity (averaged over a lead) to the bundle average velocity
μ	Fluid viscocity (lbm/hr - ft)
ρ	Fluid density (lbm/cu. ft)
ΔP_b	Average bundle pressure drop (lbf/sq. ft)
ΔP_s	Subchannel pressure drop (lbf/sq. ft)
ΔP_{s1}	Interior subchannel pressure drop (lbf/sq. ft)
$\overline{\Delta P_{s1}}$	Average interior subchannel pressure drop, defined by Eq. (B-4), (lbf/sq. ft)
ΔP_{s2}	Edge subchannel pressure drop (lbf/sq. ft)

TABLE OF CONTENTS

List of Figures

List of Tables

CHAPTER 1

INTRODUCTION

The pressure drop experiment was performed in two LMFBR blanket bundles. One of the bundles has the geometric characteristics of $\frac{P}{D}$ = 1.067 and $\frac{H}{D}$ = 8.0 which are similar to those of the blanket assemblies currently designed for the Clinch River Breeder Reactor. The second bundle has identical geomtric characteristics, except that its $\frac{H}{D}$ ratio is 4.0.

The pressure drop data were taken in two subchannels: one, a center interior subchannel and the other, a typical edge subchannel. The subchannel friction factors of the interior and edge subchannels and the bundle average friction factor are determined from the corresponding pressure drop data.

The main purpose of this experiment is to obtain information for the following hydraulic characteristics:

1) The pumping power required for the current CRBR blanket assemblies.
2) The lead length effect on the blanket bundle pressure drop.
3) The lead length effect on the local subchannel friction factors for both interior and edge subchannels.

To date, there has been no data available to aid in the understanding of the aformentioned hydraulic characteristics for the blanket assemblies. The local subchannel friction

factors for the wire wrapped hexagonal bundle are very important in determining the subchannel flow rate pattern. These parameters have not yet been introduced into the study of the hydraulic behavior of a wire-wrapped bundle. For these reasons, the experiment performed here yields fundamental information for LMFBR design practice.

CHAPTER 2

EXPERIMENTAL APPARATUS

To obtain the pressure drop data, two static pressure measurements are taken at two separate elevations by either pressure taps or instrumentation rods. The pressure taps are located in the centers of the six faces of the hexagonal bundle (as illustrated in Fig. (2-1)) to measure the edge subchannel static pressures. The instrumentation rods are made up of two parts: a hollow tube with consecutive holes of 1/32 inch diameter, and an injector which can slide inside this hollow tube and align its end hole with the tube holes. The local pressure signal is transmitted through the tube holes and the end hole located at the end of the sliding injector to a pressure gauge where the subchannel static pressure can be quantitatively determined. The design configuration of this instrumentation rod is illustrated in Fig. (2-2). Notice that two pairs of o-rings are used in the end part of the sliding rod to prevent the disturbance of the local static pressure signal from upstream or downstream static pressures. Recirculation of the subchannel fluid in the gap between the sliding rod and the tube is prevented by enclosing this gap in neoprene tubing (as shown in Fig. (2-2)). The sliding rod can be aligned with the hole (on the tube) at which the static pressure will be measured. With the aid of this instrumentation rod, the static pressure at different elevations can be determined.

The geometric characteristics of the test bundle are listed in Table (2-1). Detailed bundle design configurations and the flow loop design scheme are given in Ref. (1).

CHAPTER 3

EXPERIMENTAL RESULTS

A preliminary test is made to compare the static pressure drop data taken by two different types of instruments: pressure taps and instrumentation rods located in the assembly peripheral region (as shown in Fig. (3-1)). The results show that there is practically no difference between these two sets of data (Table (3-1) lists these two sets of data for comparison). For this reason, the edge subchannel pressure drop data are obtained in this experiment with the edge instrumentation rod. For the static pressure drop data of the interior subchannels, an instrumentation rod is placed at the center of the bundle to measure the static pressure at two different elevations. These measurements are taken at 15 inches and 27 inches below the bundle exit plane, for both interior and edge subchannels of the four inch lead length bundle. The results are illustrated in Figs. (3-1) and (3-2). For the two inch lead length bundle the static pressure data for both interior and edge subchannels are obtained at 16.1 inches and 31.1 inches below the bundle exit plane. The results are illustrated in Figs. (3-3) and (3-4) respectively. The raw data for the above four figures are documented in Appendix A.

The pressure drop data, as a function of the Reynolds number, can be determined for the interior and edge subchannels of the four and two inch lead length bundles from the above data. The pressure drop data of the two inch lead length

bundle are illustrated in Figures (3-5) and (3-6) for interior and edge subchannels respectively. The pressure drop data of the four inch lead length bundle are illustrated in Figures (3-7) and (3-8) for interior and edge subchannels respectively.

It should be noted that the pressure drop data obtained in this experiment taken on different days or by different laboratory assistants under the same nominal operating conditions are found always within the error bars presented together with the data.

CHAPTER 4

DISCUSSION OF RESULTS

The three parameters which are calculated from the experimental static pressure data will be discussed below. First, the average bundle friction factors are calculated and discussed in Sect. (4-1). Secondly, the local friction factors for the interior subchannels of both bundles are calculated and discussed in Sect. (4-2). Finally, the local friction factors for the edge subchannels of both bundles are calculated and discussed in Sect. (4-3).

4.1 Bundle Average Friction Factors

The relationship between the bundle static pressure drop and the bundle average friction factor is as follows:

$$\Delta P_b = f_b \frac{L}{De} \frac{\rho \bar{V}_b^2}{2g_c} \qquad (4\text{-}1)$$

where ΔP_b = bundle average pressure drop over subchannel length L

f_b = bundle average friction factor

De = bundle average equivalent hydraulic diameter

ρ = fluid density

V_b = bundle average velocity.

From the above formula, the bundle average friction factor can be reduced provided that ΔP_b is known. In this experiment, ΔP_b is simply determined by averaging the

the pressure drop data for interior and edge subchannel as follows:

$$\Delta P_b = \frac{N_1 A_1 \Delta P_1 + \Delta P_2 A_2 N_2}{N_1 A_1 + N_2 A_2} \qquad (4\text{-}2)$$

where N_1 = number of interior subchannels

N_2 = number of edge subchannels.

It should be noted that the ΔP_b can be determined by a force balance in the following way:

$$\Delta P_b = \frac{\sum_{i=\text{subchannel}}^{N} \Delta P_i A_i}{A_b} \qquad (4\text{-}3)$$

where ΔP_i = pressure drop for subchannel i

A_i = area for subchannel i

A_b = total bundle area

N = total number of subchannels

provided the pressure drop data are available for all the subchannels over a certain subchannel length. The simplification made in Eq. (4-2) is based on the assumption of constant static pressure drops for all the interior subchannels and constant static pressure drops for all the edge subchannels. However, since the static pressure drop for an interior subchannel is very close in magnitude to that for an edge subchannel (within ±6% difference as can be observed by comparing Figs. (3-5) with (3-6), and (3-7) with (3-8)), the simplification made in Eq. (4-2) will not involve a large error in the determination of ΔP_b.

From Eqs. (4-1) and (4-2), the bundle average friction factor can be calculated from the data presented in Chapter 3.

Figure (4-1) shows the calculated bundle average friction factor for the four inch lead length bundle. Figure (4-2) shows the calculated bundle average friction factor for the two inch lead length bundle. In these two figures, Rehme's correlation (Ref. 2) and Novendstern's correlation (Ref. 3) are plotted against the data for comparison.

It can be concluded from these two figures that

1) In the high turbulent flow regime, i.e., Re > 7000, the bundle average friction factors are proportional to $Re^{-0.25}$ for both two and four inch lead bundles. These two bundle average friction factors are characterized by the following two formulas:

$$f_b = \frac{0.48}{Re^{0.25}} \quad \text{for the four inch lead bundle} \qquad (4-4)$$

$$f_b = \frac{0.9}{Re^{0.25}} \quad \text{for the two inch lead bundle} \qquad (4-5)$$

2) The friction factors become inversely proportional to the Reynolds number in the flow regime below Re = 500 for both bundles. These laminar bundle average friction factors are characterized as:

$$f_b = \frac{90}{Re} \quad \text{for the four inch lead bundle} \qquad (4-6)$$

$$f_b = \frac{160}{Re} \quad \text{for the two inch lead bundle} \qquad (4-7)$$

3) In the flow regime with Re between 500 and 7000 the bundle average friction factors possess the characteristics of both the high turbulent and the pure laminar flow

regime bundle average friction factors. In other words, the bundle average friction factors are proportional to Re^{-n}, where n is a number between 0.25 and 1.0.

4) Novendstern's correlation predicts bundle average friction factors which are higher than those obtained experimentally for both two and four inch lead bundles. The difference in Novendstern's results and the experiment results is explained by noting the applicable range for Novendstern's correlation with the experimental geometric condition. Since the geometric conditions for the two inch lead bundle are outside the applicable range of rod diameter and the $\frac{H}{D}$ ratio,and for the four inch lead bundle, are outside the applicable range of rod diameter, a difference in results should be expected.

5) Rehme's correlation predicts the bundle average friction factors which are lower than those obtained in this experiment for both two and four inch lead bundles. The reason for the difference between the predictions of the correlation and the experimental results is that the correlation was determined for the $\frac{P}{D}$ ratios of 1.125 to 1.417. The error bar illustrated in Figs. (4-1) and (4-2) is the maximum expected error inherent in the determination of the bundle average friction factors. The deviation of this maximum expected error is given in Appendix B.

4.2 Local Friction Factors of Interior Subchannels

The local friction factor is related to the subchannel pressure drop as follows:

$$\Delta P_s = f_s \frac{L}{Des} \frac{\rho V_s^2}{2} \qquad (4-8)$$

where ΔP_s = subchannel pressure drop for either interior or edge subchannel

f_s = local subchannel friction factor

Des= subchannel equivalent hydraulic diameter

V_s = subchannel average velocity (over one lead length)

The parameter ΔP_s is measured in this experiment and the parameter V_s is determined by the flow split parameters x_1 and x_2 (Ref. 4), defined as the ratios of the average interior subchannel velocity to the bundle average velocity, measured in both two inch and four inch lead bundles. By using the above equation and the measured parameters ΔP_{s1} (interior subchannel pressure drop) and x_1, we can calculate the local subchannel friction factors of the interior subchannels for both two and four inch lead bundles. The calculation results are illustrated in Figs. (4-3) and (4-4) for the four and two inch lead bundles respectively. It should be noted that in these two figures the local interior subchannel friction factors are plotted against the local interior subchannel Reynolds number, which is defined as:

$$Re_1 = \frac{\rho V_1 De_1}{\mu} \qquad (4-9)$$

where V_1 = interior subchannel average velocity = $x_1 V_b$

De = interior subchannel equivalent hydraulic diameter.

From the above two figures, the following hydraulic characteristics are observed for the local interior subchannel friction factors:

1) In the high turbulent flow regime, i.e., $Re_1 > 7000$, the local interior subchannel friction factors are proportional to $Re_1^{-0.25}$ for both two and four inch bundles. These two interior subchannel turbulent friction factors are characterized by the following formulas:

$$f_{s1} = \frac{0.593}{Re_1^{0.25}} \quad \text{for the four inch lead bundle} \qquad (4\text{-}10)$$

$$f_{s1} = \frac{1.27}{Re_1^{0.25}} \quad \text{for the two inch lead bundle} \qquad (4\text{-}11)$$

2) The local interior subchannel friction factor for the two inch lead bundle is larger than that for the four inch lead bundle throughout the Reynolds number range under investigation.

4.3 Local Friction Factors of Edge Subchannels

The local friction factors of the edge subchannels are calculated according to Eq. (4-8) by employing the edge subchannel pressure drop data obtained in this experiment and the edge subchannel flow split parameters x_2 reported in Ref. (4) for both two and four inch lead bundles. The results

are illustrated in Figs. (4-5) and (4-6) for the four and two inch lead bundles. In these two figures, f_{s2} (local edge subchannel friction factor) is plotted against the local edge subchannel Reynolds number which is defined as:

$$Re_2 = \frac{\rho V_2 De_2}{\mu} . \qquad (4\text{-}12)$$

The maximum expected errors illustrated in the above figures as error bars are derived in Appendix B.

From the above two figures, we can observe the following hydraulic characteristics:

1) In the high turbulent flow regime, i.e., $Re_2 > 7000$, the local edge subchannel friction factors are proportional to $Re_2^{-0.25}$ for both two and four inch lead bundles. These two sets of the local edge subchannel friction factor results are correlated:

$$f_{s2} = \frac{0.39}{Re_2^{0.25}} \text{ for the four inch lead bundle} \qquad (4\text{-}13)$$

$$f_{s2} = \frac{0.6}{Re_2^{0.25}} \text{ for the two inch lead bundle} \qquad (4\text{-}14)$$

Comparing these two formulas with Eqs. (4-10) and (4-11), we can conclude that the wire wrap lead length has a stronger effect on the interior subchannel friction factor than on the edge subchannel friction factor.

2) The local edge subchannel friction factor for the two inch lead bundle is always larger than that for the four inch lead bundle.

CHAPTER 5

CONCLUSION

The experiment results in this report has shown the following general characteristics concerning the bundle and subchannel friction factors of the test blanket mock-ups:

1. The turbulent friction factors either for two types of subchannels, i.e., edge and interior, or for the bundle as a whole are proportional to $Re^{-0.25}$.
2. The edge subchannel friction factors are considerably lower than the interior subchannel friction factors over the Reynolds number range from laminar flow to turbulent flow.
3. Current bundle friction factor correlations developed either by Novendstern or by Rheme be extended to the experimental results within the experimental error bar.

A subchannel pressure drop model which explain the above general characteristic (2) has been developed by C. Chiu et al, in Reference 5. This model considers the effect of the form drag, induced by the wire, and the transverse velocity between subchannels in the determination of the subchannel friction factor. Further work to extend this model to predict the bundle average friction factor is under way by C. Chiu and Kerry Basehore.

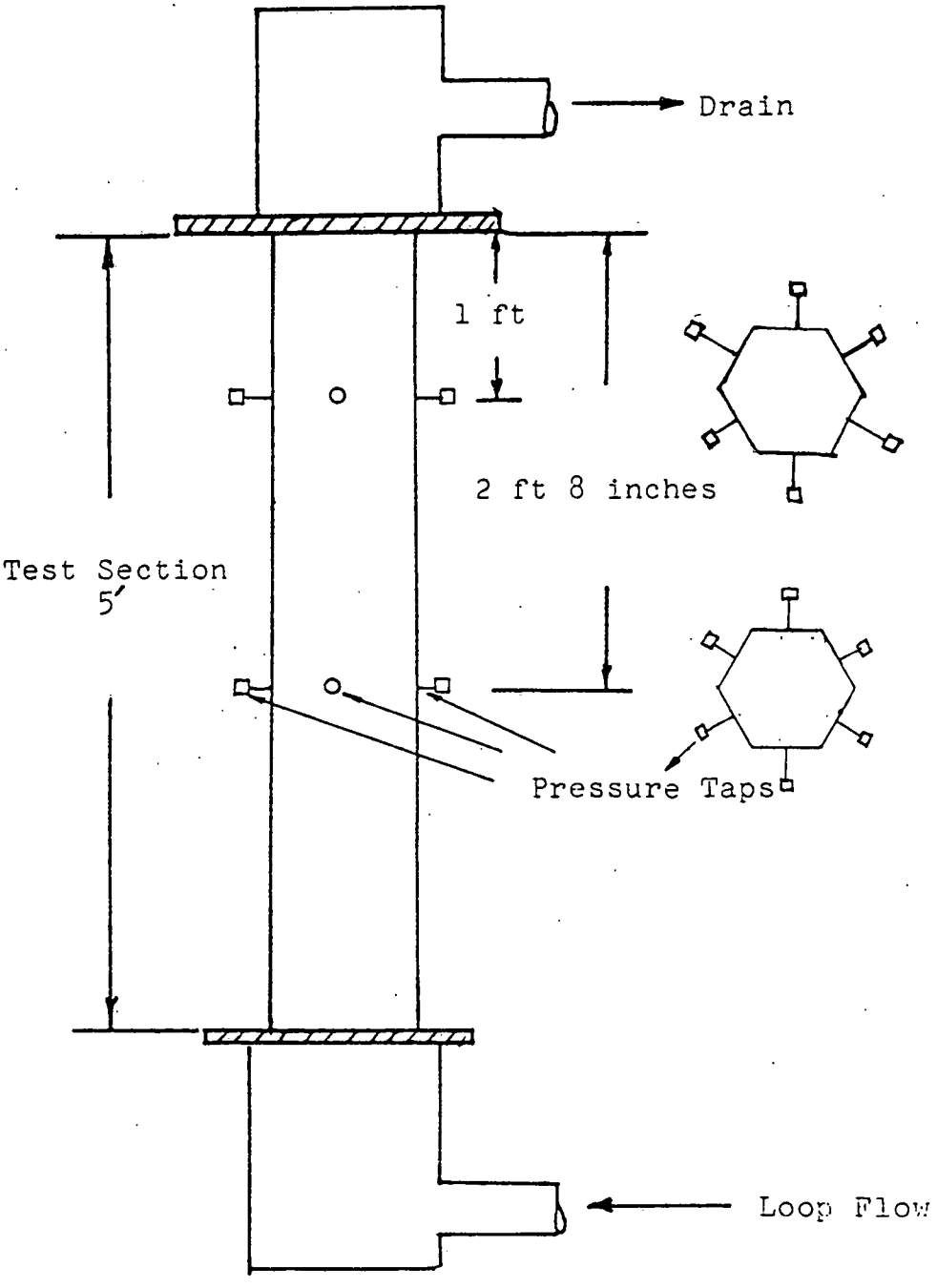

FIGURE 2-1 Static Pressure Tap Location Scheme

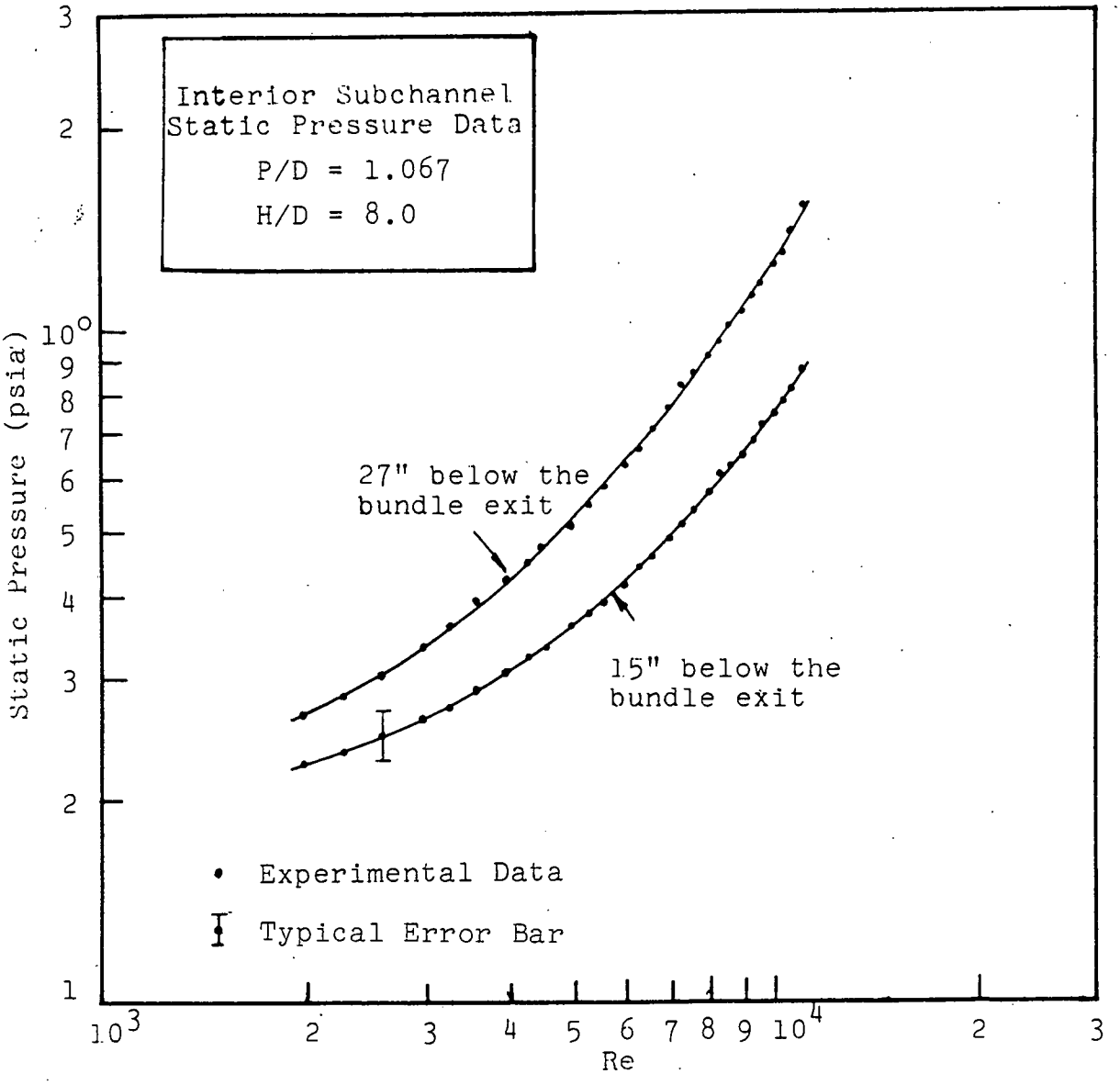

FIGURE 3-1 Static Pressures at 15" and 27" Below the Exit Plane of the 4" Lead Bundle (Interior Subchannel)

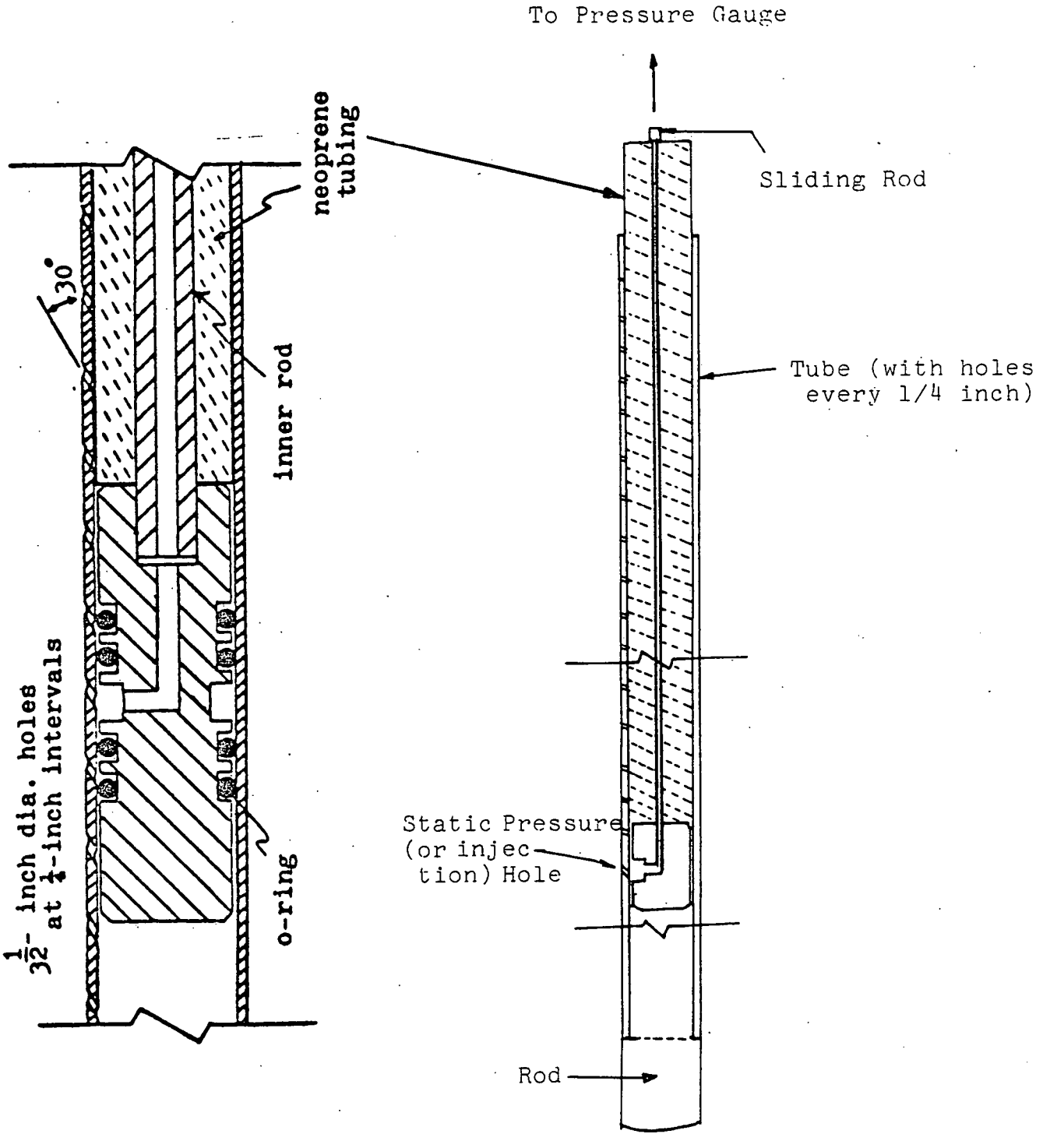

FIGURE 2-2 Design Configuration of Instrumentation Rod

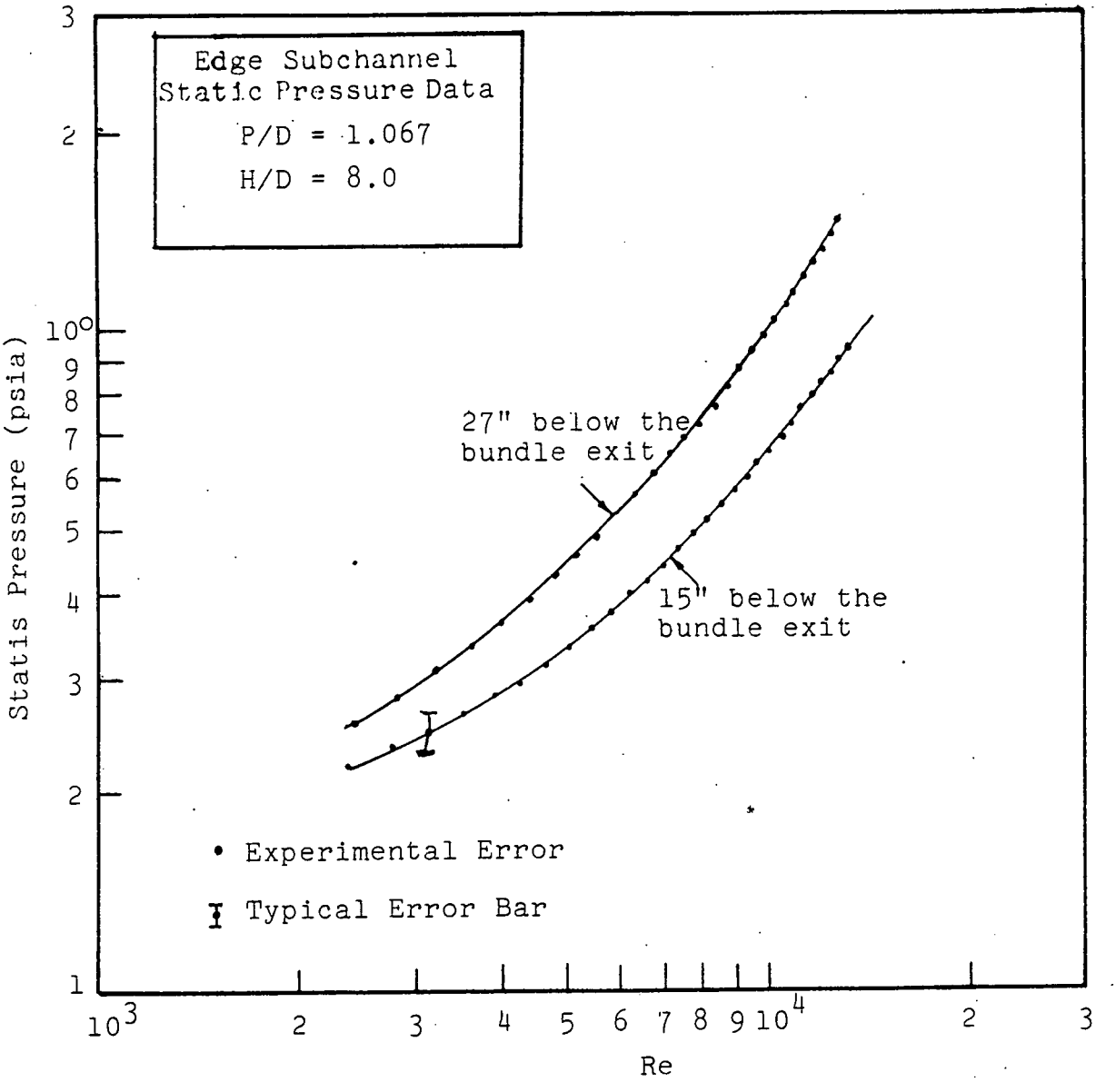

FIGURE 3-2 Static Pressures at 15" and 27" Below the Exit Plane of the 4" Lead Bundle (Edge Subchannel)

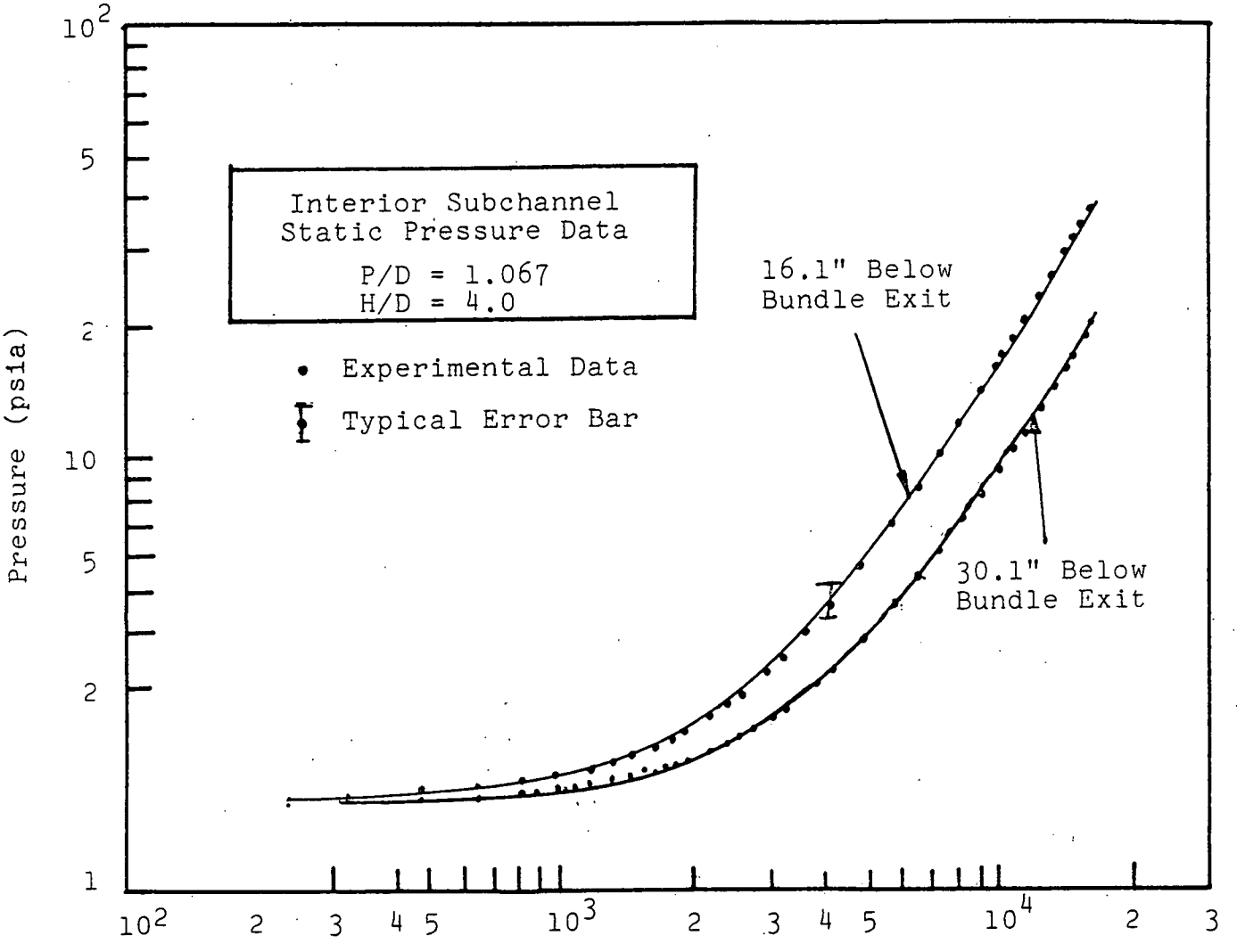

FIGURE 3-3 Static Pressures at 16.1" and 30.1" Below the Exit Plane of the 2" Lead Bundle (Interior Subchannel)

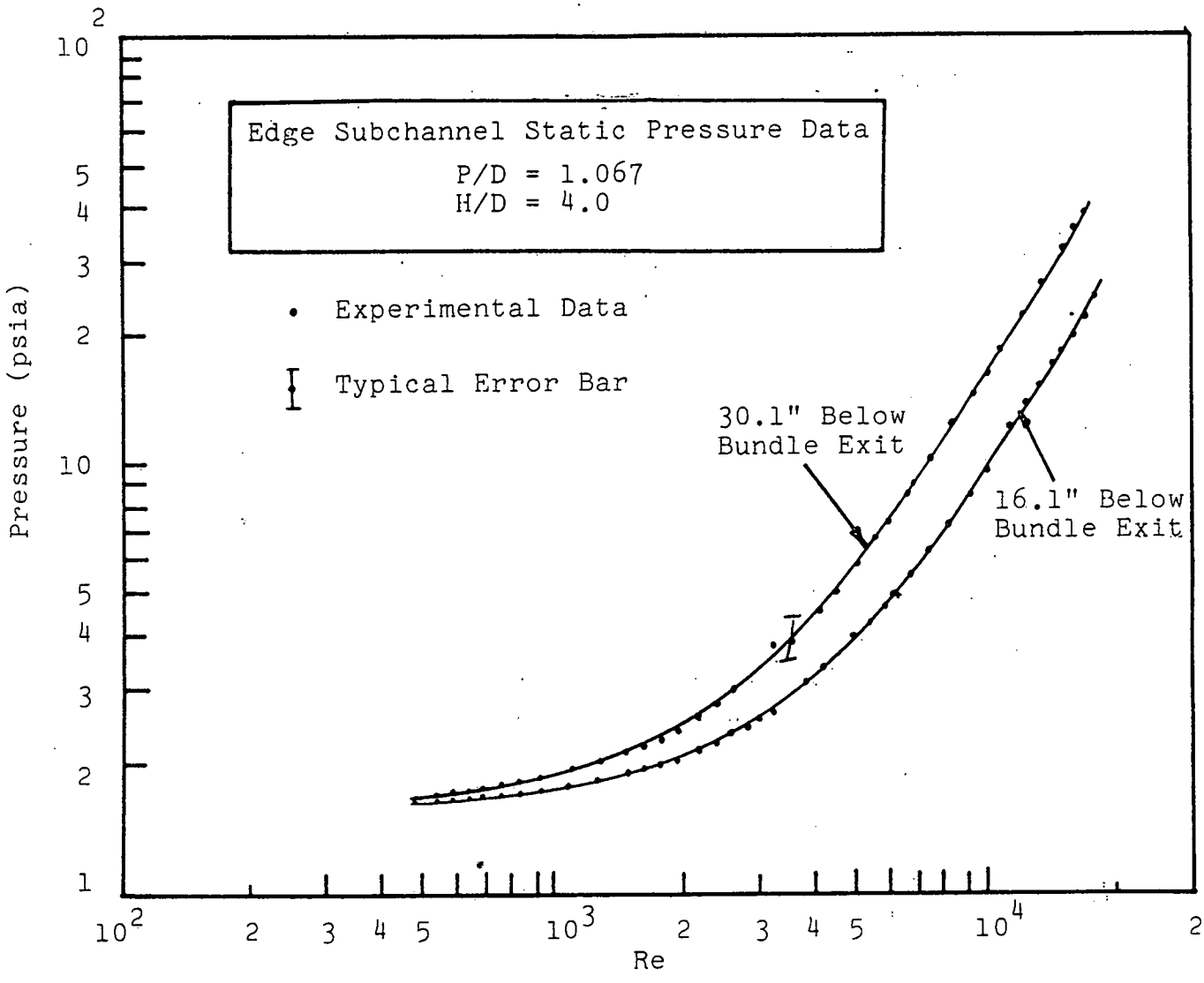

FIGURE 3-4 Statis Pressures at 16.1" and 30.1" Below the Exit Plane of the 2" Lead Bundle (Edge Subchannel)

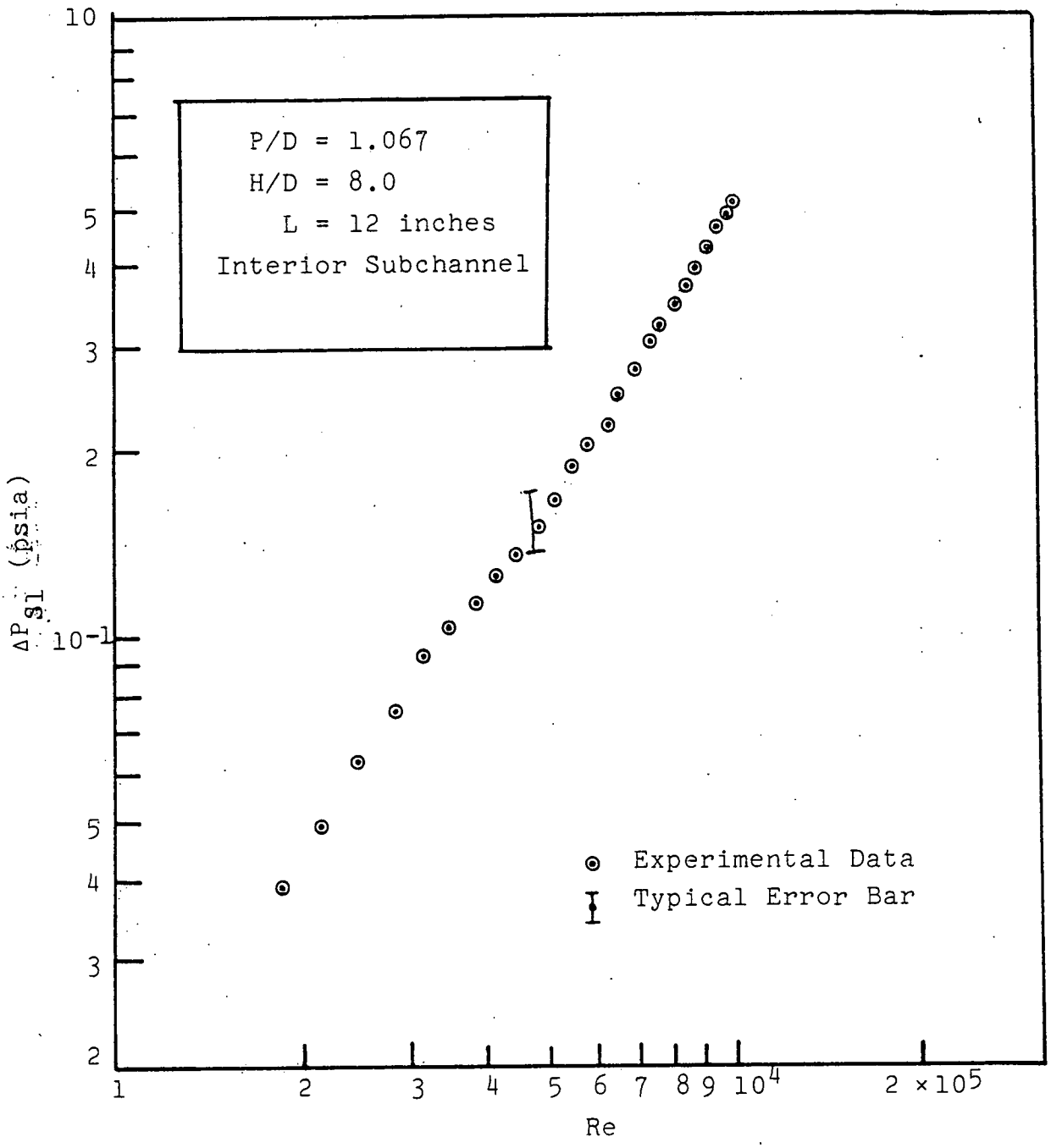

FIGURE 3-5 Pressure Drop Data of an Interior Subchannel in the 4" Lead Bundle

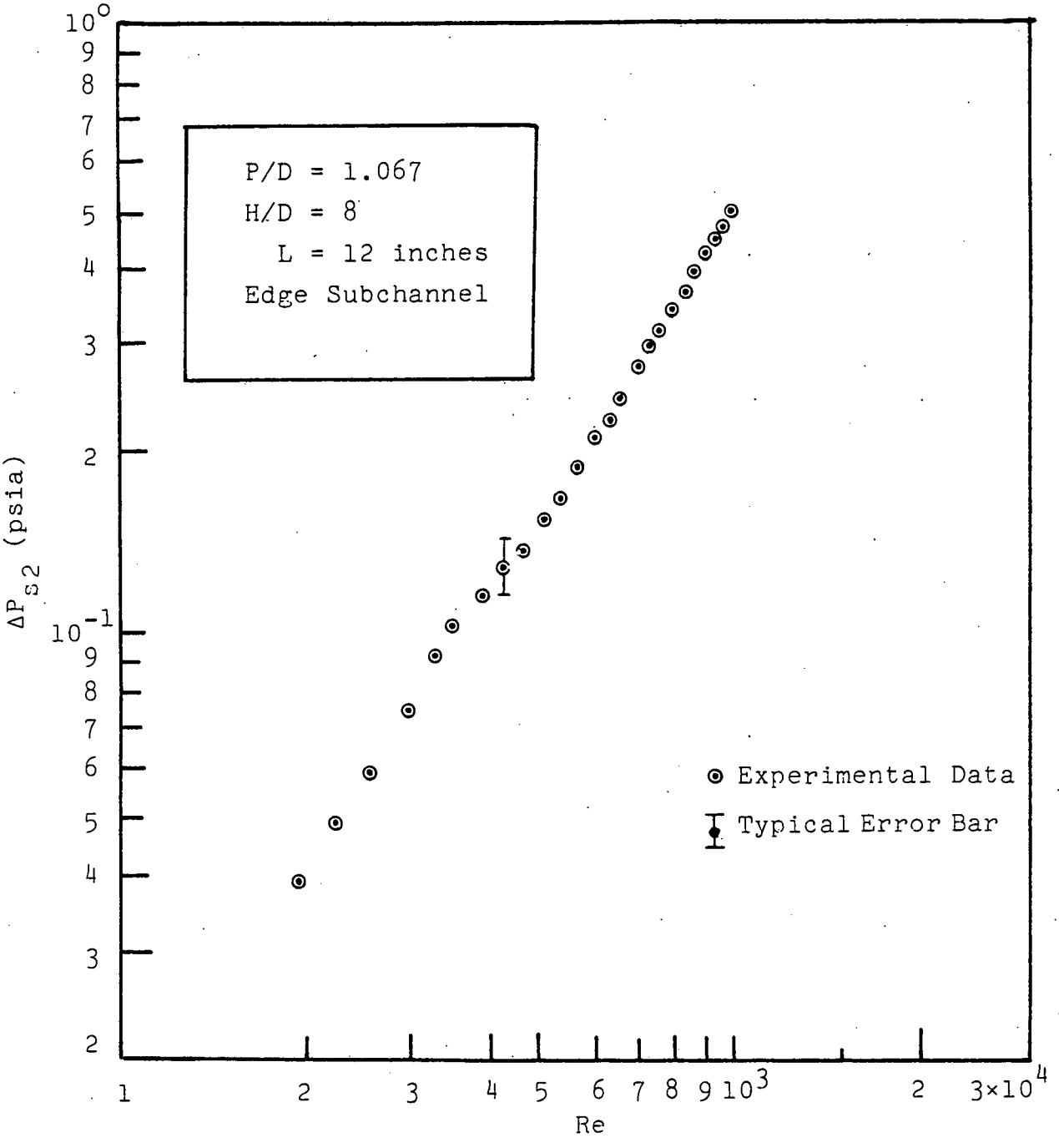

FIGURE 3-6 Pressure Drop Data of Edge Subchannel in the 4" Lead Bundle

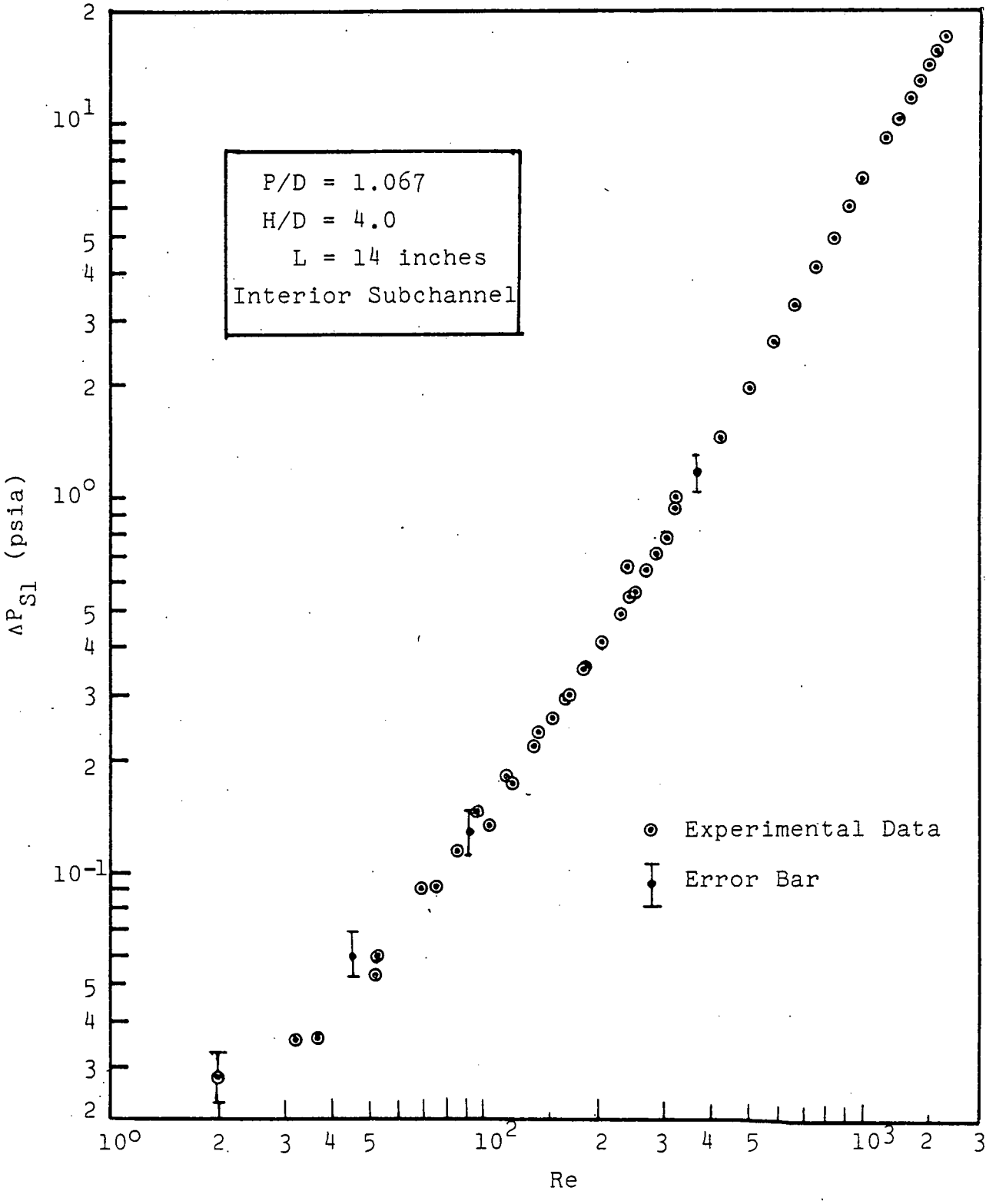

FIGURE 3-7 Pressure Drop Data of an Interior Subchannel in the 2" Lead Bundle

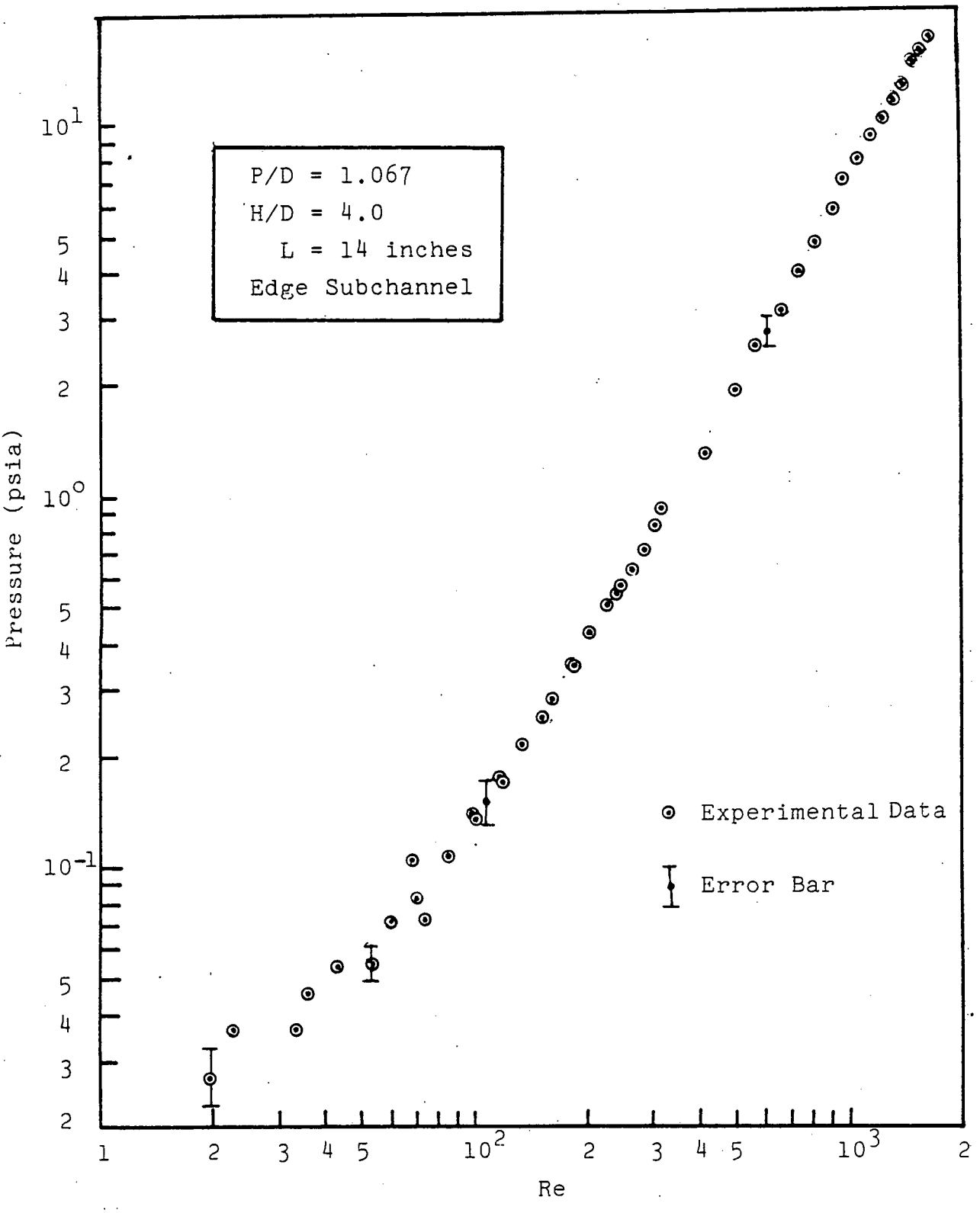

FIGURE 3-8 Pressure Drop Data of an Edge Subchannel in the 2" Lead Bundle

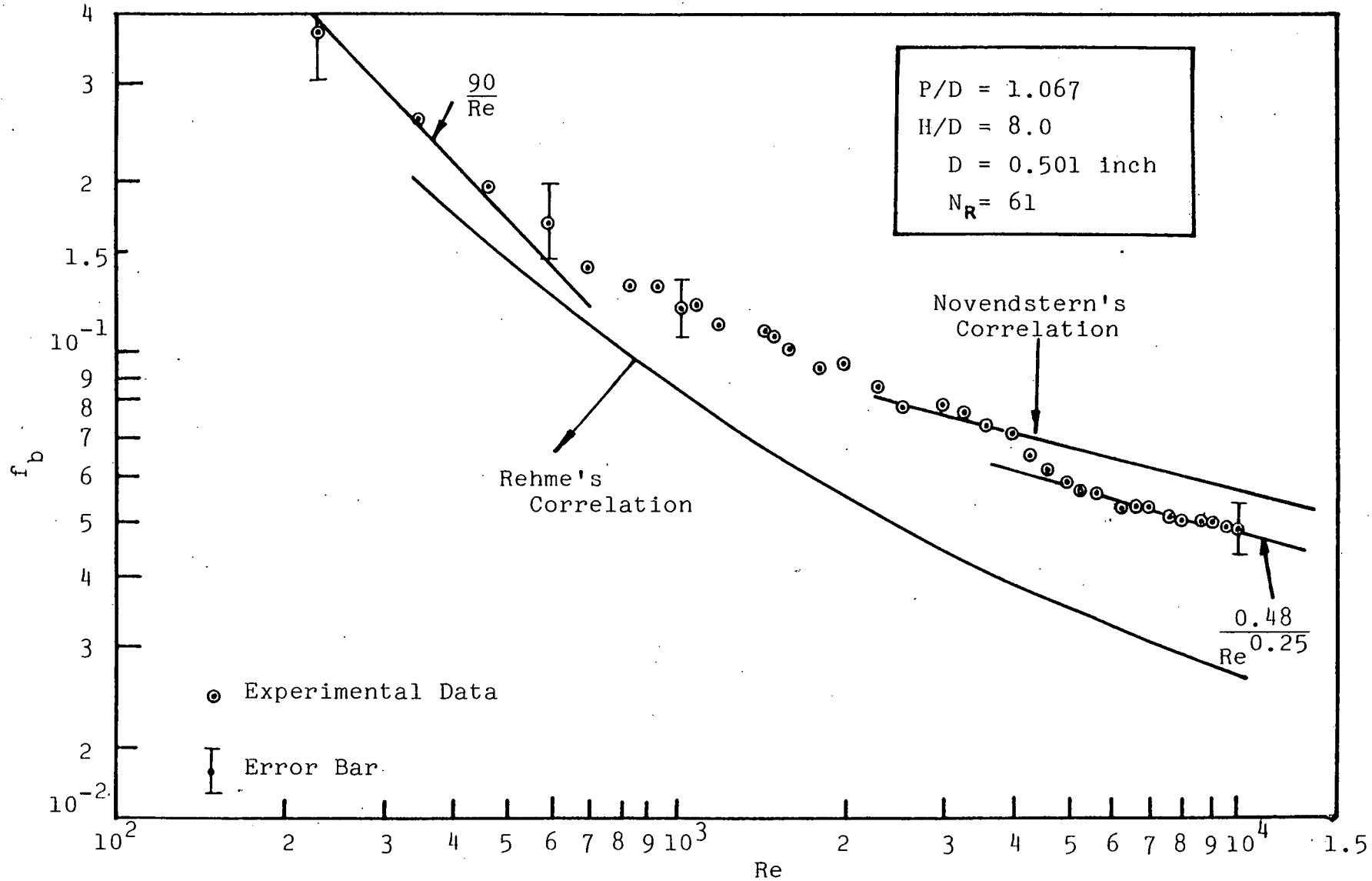

FIGURE 4-1 Bundle Average Friction Factor for the 4" Lead Bundle

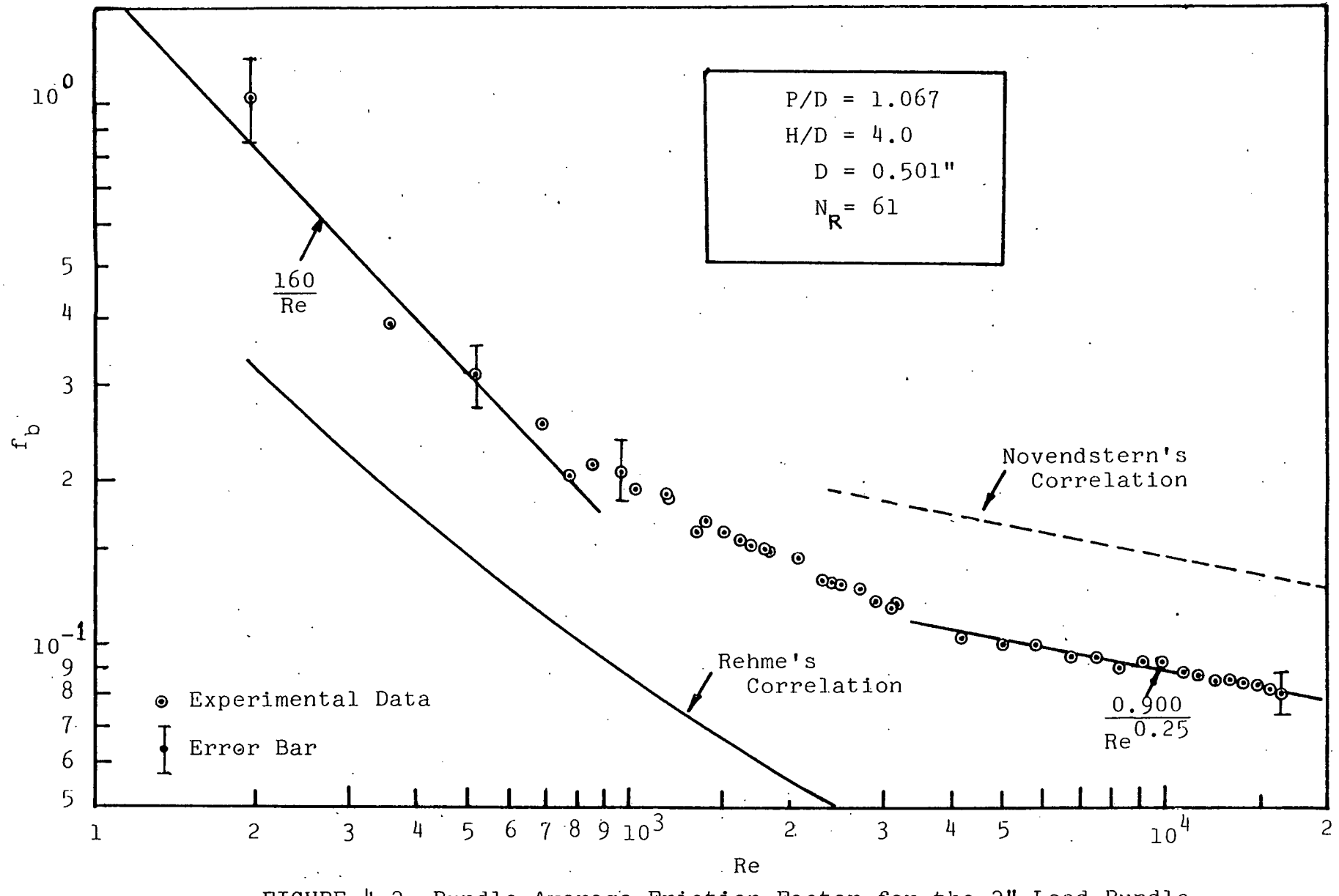

FIGURE 4-2 Bundle Average Friction Factor for the 2" Lead Bundle

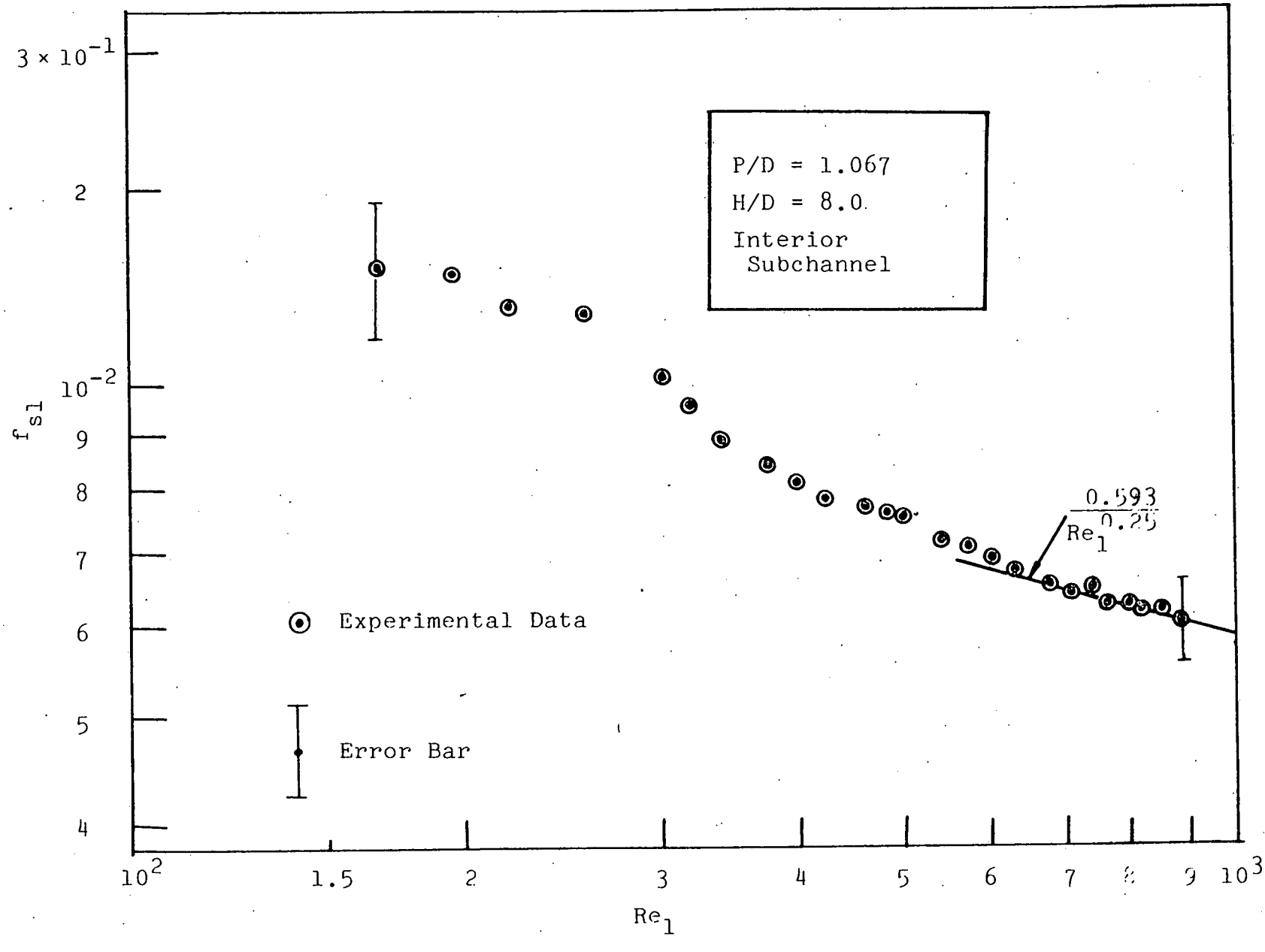

FIGURE 4-3 Local Interior Subchannel Friction Factor for the 4" Lead Bundle

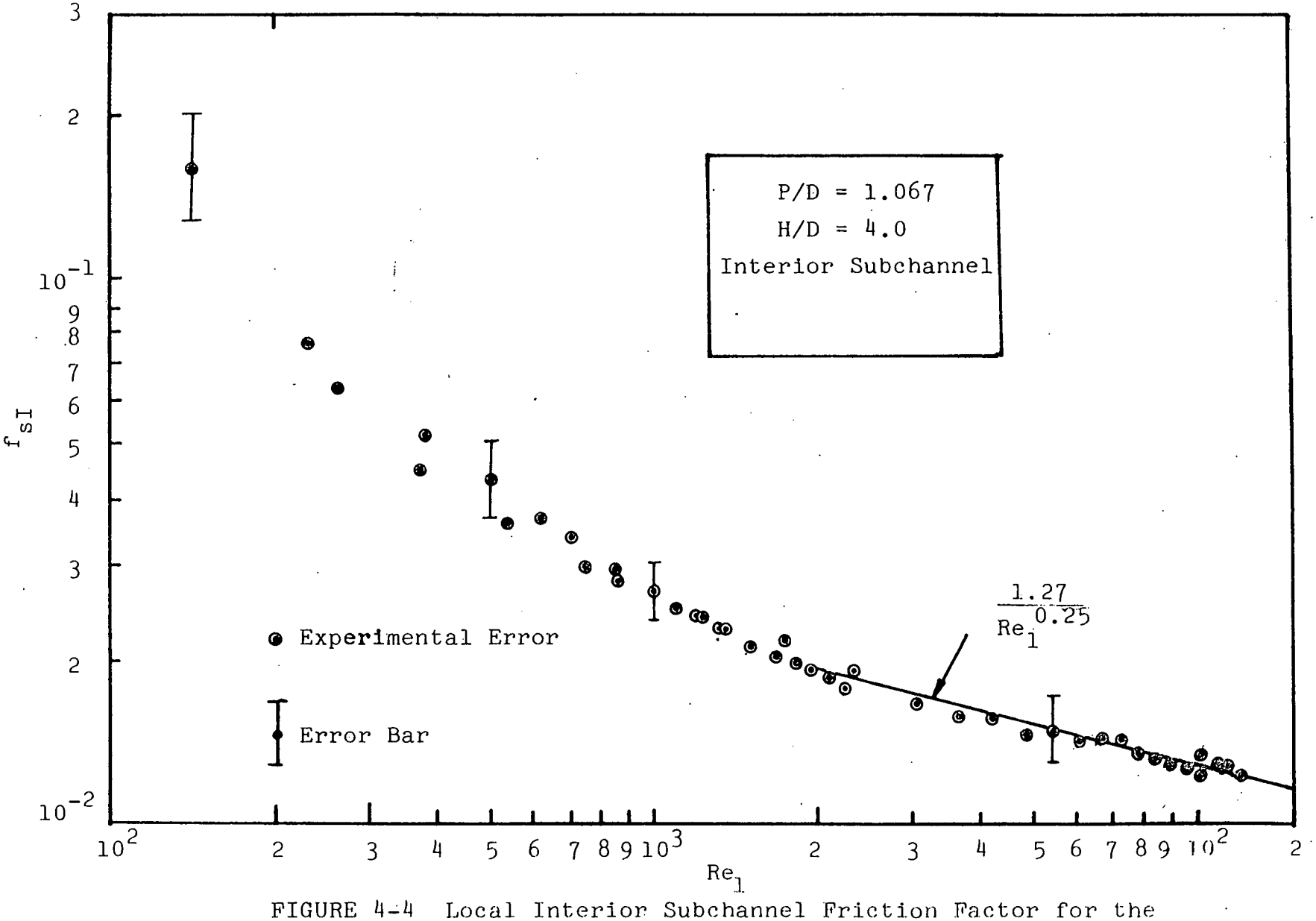

FIGURE 4-4 Local Interior Subchannel Friction Factor for the 2" Lead Bundle

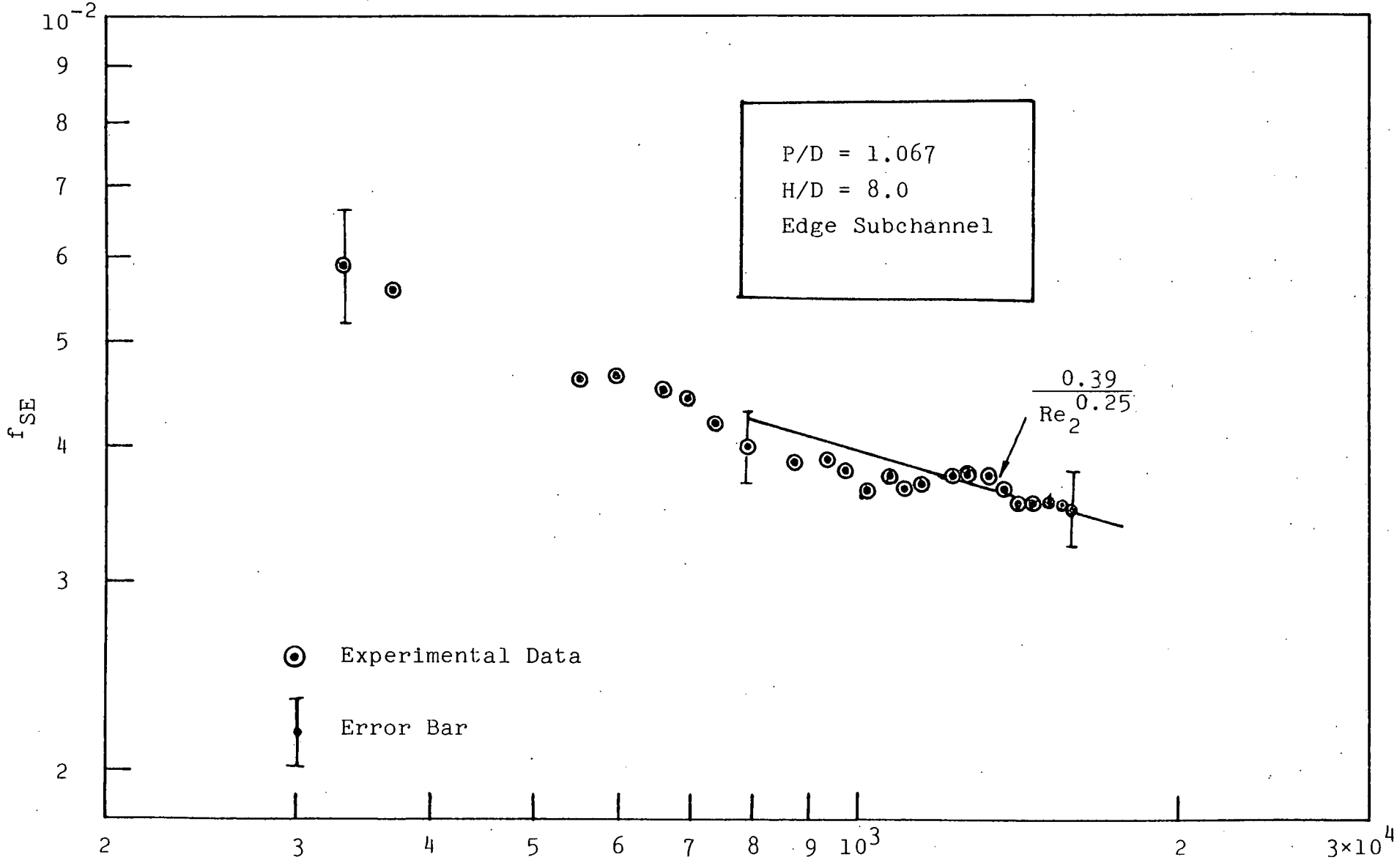

FIGURE 4-5 Local Edge Subchannel Friction Factor for the 4" Lead Bundle

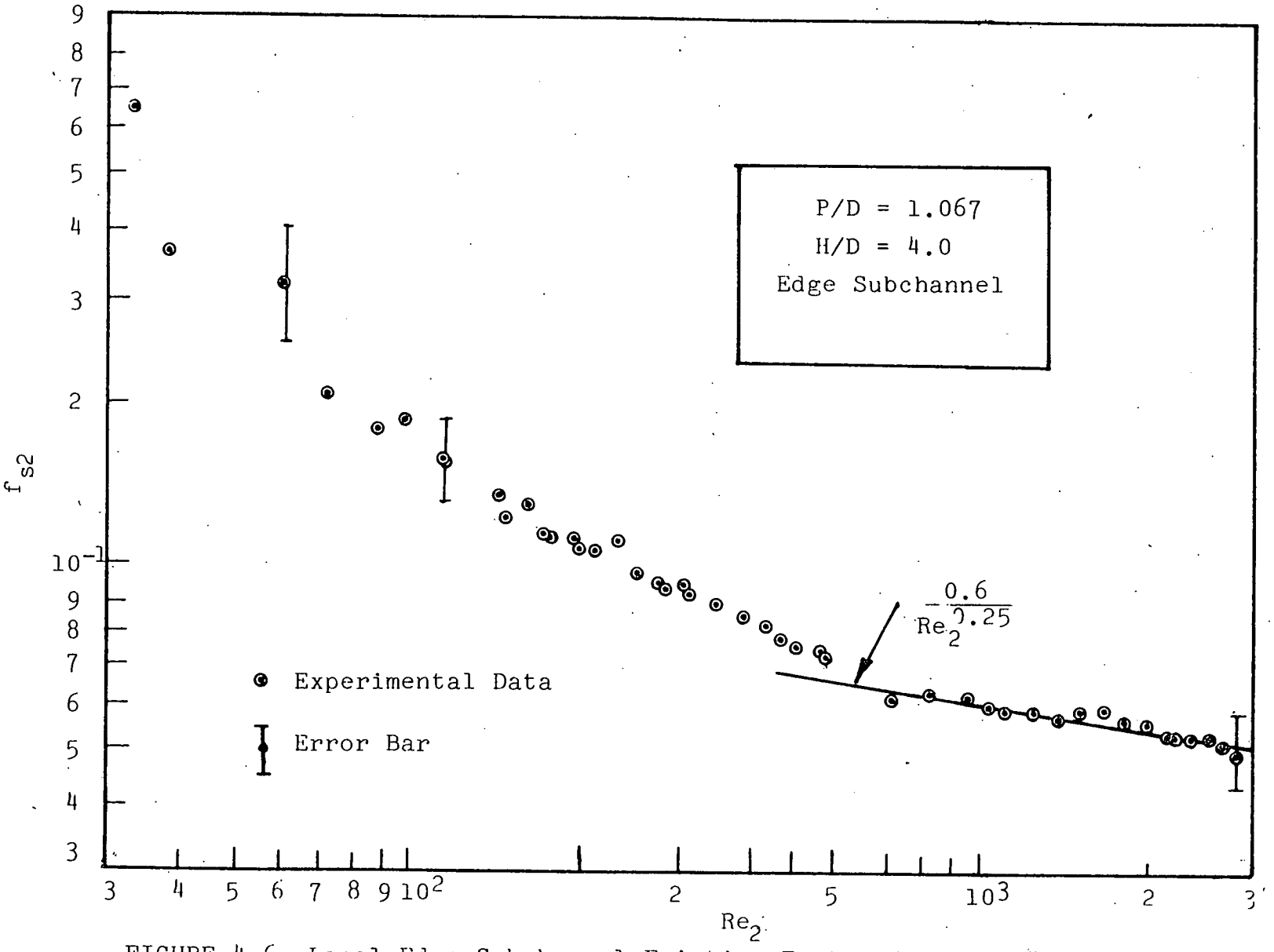

FIGURE 4-6 Local Edge Subchannel Friction Factor for the 2" Lead Bundle

TABLE 2-1

As-Built Test Bundle Geometric Parameters

Bundle Length	60 inches
Flat-to-Flat Distance (three directions)	4.275 inches
Rod Diameter	0.5011 inch
Wire Diameter	0.0314
Wire Wrap Lead	4.0 inch
Face Width (six faces)	2.468 inches
Average F-Factor	0.820

TABLE 3-1

List of Pressure Drop Data of Pressure Taps and Instrumentation Rod (4" Wire Lead Bundle)

Re	ΔP_{tap} (inch of H_2O)	$\Delta P_{Inst.Rod}$ (inch of H_2O)	Difference %
470	3.87	3.80	1.8%
1100	7.92	8.15	2.8%
1900	16.2	16.0	1.25%
3300	40.8	41.0	0.5%
4600	64.9	65.1	0.3%
5600	85.17	86.7	1.76%
6300	101.8	102.1	0.3%
7300	131.9	133.1	1.0%
8300	163.7	163.0	0.4%
9300	196.7	197.0	0.1%
10000	220.45	222.3	1.85%

Note : all the static Pressure data are measured in inch of water

ΔP_{tap} = Average Pressure Drop of Six Faces Measured by Pressure Taps

$$\text{Difference} = \left| \frac{\Delta P_{tap} - \Delta P_{Inst.Rod}}{\Delta P_{Inst.Rod}} \right|$$

APPENDIX A

LIST OF DATA

TABLE A-1

STATIC PRESSURE DATA FOR THE TWO INCH LEAD BUNDLE (INTERIOR SUBCHANNEL)

GPM	RE	P_{static}(30.1")	P_{static}(16.1")
3.70	197	1.69	1.66
5.18	322	1.71	1.68
5.55	362	1.72	1.69
7.40	517	1.77	1.71
7.40	528	1.77	1.71
9.25	693	1.82	1.73
10.0	744	1.86	1.77
11.1	858	1.89	1.77
12.6	972	1.95	1.80
13.0	1030	1.95	1.81
14.8	1170	2.06	1.88
14.8	1190	2.02	1.85
16.7	1360	2.11	1.90
17.4	1390	2.17	1.93
18.5	1520	2.20	1.95
20.0	1630	2.29	2.00

TABLE A-1 (cont'd)

GPM	RE	P_{static}(30.1")	P_{static}(16.1")
20.4	1690	2.28	1.98
22.2	1810	2.42	2.08
22.2	1850	2.39	2.05
25.2	2080	2.60	2.18
27.8	2300	2.76	2.27
30	2400	3.07	2.42
30.0	2500	2.92	2.35
32.2	2690	3.07	2.42
34.8	2880	3.25	2.54
37.0	3110	3.43	2.65
40	3200	3.84	2.84
50	4200	4.85	3.39
60	5000	6.01	4.06
70	5800	7.36	4.76
80	6700	8.81	5.59
90	7500	10.5	6.42

TABLE A-1 (cont'd)

GPM	RE	P_{static}(30.1")	P_{static}(16.1")
100	8340	12.3	7.36
110	9190	14.5	8.55
120	10000	16.7	9.65
130	10800	19.0	11.1
140	11500	21.7	12.5
150	12400	24.4	14.1
160	13200	27.2	15.6
170	14100	30.2	17.2
180	14900	33.1	18.8
190	15800	36.4	20.6
200	16600	39.4	22.3

TABLE A-2

STATIC PRESSURE DATA FOR THE TWO INCH LEAD BUNDLE (EDGE SUBCHANNEL)

GPM	RE	P_{static}(30.1")	P_{static}(16.1")
3.70	197	1.69	1.66
4.44	227	1.61	1.59
5.55	313	1.73	1.70
5.55	362	1.72	1.68
7.03	428	1.71	1.77
7.40	528	1.77	1.71
8.14	591	1.80	1.73
10.36	685	1.88	1.77
9.25	693	1.81	1.73
10.0	744	1.84	1.77
11.1	858	1.88	1.77
12.95	885	1.96	1.81
12.6	972	1.95	1.80
13.0	1030	1.94	1.80
15.54	1086	2.08	1.88
14.8	1170	2.04	1.86

TABLE A-2 (cont'd)

GPM	RE	P_{static}(30.1")	P_{static}(16.1")
14.8	1190	2.01	1.84
18.00	1276	2.21	1.95
16.7	1360	2.09	1.88
17.4	1390	2.17	1.91
18.5	1520	2.18	1.93
20.0	1630	2.27	1.98
20.4	1690	2.27	1.98
22.2	1810	2.42	2.06
22.2	1850	2.36	2.02
25.2	2080	2.58	2.15
27.8	2300	2.74	2.24
30	2400	2.85	2.31
30.0	2500	2.89	2.31
32.2	2690	3.05	2.42
34.8	2880	3.23	2.53
37.0	3110	3.43	2.62

TABLE A-2 (cont'd)

GPM	RE	P_{static}(30.1")	P_{static}(16.1")
40	3200	3.64	2.71
50	4200	4.55	3.25
60	5000	5.77	3.86
70	5800	7.11	4.58
90	7500	10.2	6.24
100	8340	12.0	7.22
110	9190	14.1	8.16
120	10000	16.3	9.20
130	10800	18.6	10.4
140	11500	21.0	11.7
150	12400	23.4	13.1
160	13200	26.3	14.7
170	14100	29.2	16.3
180	14900	32.3	17.8
190	15800	35.1	19.4
200	16600	37.5	20.6

TABLE A-3

STATIC PRESSURE DATA FOR THE FOUR INCH LEAD BUNDLE (INTERIOR SUBCHANNEL)

GPM	RE	P_{static}(27")	P_{static}(15")
30	2000	2.67	2.24
35	2300	2.85	2.35
40	2600	3.07	2.49
45	3000	3.36	2.63
50	3300	3.64	2.74
55	3600	3.93	2.89
60	4000	4.22	3.07
65	4300	4.51	3.25
70	4600	4.76	3.39
75	5000	5.12	3.61
80	5300	5.49	3.79
85	5600	5.88	3.97
90	6000	6.32	4.19
95	6300	6.68	4.44
100	6600	7.15	4.62
105	7000	7.69	4.91

TABLE A-3 (cont'd)

GPM	RE	P_{static}(27")	P_{static}(15")
110	7300	8.19	5.16
115	7600	8.66	5.45
120	8000	9.20	5.77
125	8300	9.74	6.06
130	8600	10.29	6.32
135	9000	10.83	6.57
140	9300	11.48	6.89
145	9600	11.95	7.22
150	10000	12.63	7.58
155	10300	13.35	7.87
160	10600	14.15	8.34
165	11000	15.45	8.81

TABLE A-4

STATIC PRESSURE DATA FOR THE FOUR INCH LEAD BUNDLE (EDGE SUBCHANNEL)

GPM	RE	P_{static}(27")	P_{static}(15")
30	2000	2.53	2.20
35	2300	2.74	2.35
40	2600	3.00	2.49
45	3000	3.28	2.63
50	3300	3.57	2.78
55	3600	3.86	2.92
60	4000	4.15	3.10
65	4300	4.47	3.28
70	4600	4.76	3.54
75	5000	5.20	3.72
80	5300	5.52	3.97
85	5600	5.92	4.15
90	6000	6.35	4.37
95	6300	6.68	4.62
100	6600	7.00	4.84
105	7000	7.47	5.09

TABLE A-4 (cont'd)

GPM	RE	P_{static}(27")	P_{static}(15")
110	7300	8.01	5.38
115	7600	8.44	5.70
120	8000	8.95	5.95
125	8300	9.49	6.24
130	8600	10.10	6.50
135	9000	10.61	6.82
140	9300	11.12	7.15
145	9600	11.73	7.54
150	10000	12.27	7.90
155	10300	12.88	8.26
160	10600	13.53	8.55
165	11000	14.22	8.91

TABLE A-5

SUBCHANNEL PRESSURE DROP DATA FOR THE TWO INCH LEAD BUNDLE (INTERIOR SUBCHANNEL)

GPM	RE	ΔP_{SI}
3.70	197	0.0271
5.18	322	.0361
5.55	362	.0361
7.40	517	.0541
7.40	528	.0632
9.25	693	.0902
10.0	744	.0902
11.1	858	.117
12.6	972	.144
13.0	1030	.135
14.8	1170	.180
14.8	1190	.171
16.7	1360	.208
17.4	1390	.235
18.5	1520	.253
20.0	1630	.289
20.4	1690	.298

TABLE A-5 (cont'd)

GPM	RE	ΔP_{SI}
22.2	1810	.343
22.2	1850	.343
25.2	2080	.415
27.8	2300	.487
30	2400	.65
30.0	2500	.559
32.2	2690	.632
34.8	2880	.704
37.0	3110	.776
40	3200	1.00
50	4200	1.46
60	5000	1.95
70	5800	2.60
80	6700	3.22
90	7500	4.1
100	8340	4.9
110	9190	6.0

TABLE A-5 (cont'd)

GPM	RE	ΔP_{SI}
120	10000	7.1
130	10800	7.9
140	11500	9.2
150	12400	10.3
160	13200	11.6
170	14100	13.0
180	14900	14.3
190	15800	15.8
200	16600	17.1

TABLE A-6

SUBCHANNEL PRESSURE DROP DATA FOR THE TWO INCH LEAD BUNDLE (EDGE SUBCHANNEL)

GPM	RE	ΔP_{SE}
3.70	197	0.0271
4.44	227	.0361
5.55	313	.0361
5.55	362	.0451
7.03	428	.0541
7.40	528	.0541
8.14	591	.0722
10.36	685	.108
9.25	693	.0812
10.0	744	.0722
11.1	858	.108
12.95	885	.144
12.6	972	.144
13.0	1030	.135
15.54	1086	.198
14.8	1170	.180
14.8	1190	.171

TABLE A-6 (cont'd)

GPM	RE	ΔP_{SE}
18.00	1276	.262
16.7	1360	.217
17.4	1390	.253
18.5	1520	.253
20.0	1630	.289
20.4	1690	.298
22.2	1810	.361
22.2	1850	.343
25.2	2080	.433
27.8	2300	.505
30	2400	.54
30.0	2500	.577
32.2	2690	.632
34.8	2880	.704
37.0	3110	.812
40	3200	.93
50	4200	1.30

TABLE A-6 (cont'd)

GPM	RE	ΔP_{SE}
60	5000	1.91
70	5800	2.53
80	6700	3.17
90	7500	4.0
100	8340	4.8
110	9190	5.9
120	10000	7.1
130	10800	8.2
140	11500	9.3
150	12400	10.3
160	13200	11.6
170	14100	12.9
180	14900	14.5
190	15800	15.7
200	16600	16.9

TABLE A-7

SUBCHANNEL PRESSURE DROP DATA FOR THE FOUR INCH LEAD BUNDLE (INTERIOR SUBCHANNEL)

GPM	RE	ΔP_{SI}
30	2000	0.397
35	2300	.496
40	2600	.614
45	3000	.758
50	3300	.938
55	3600	1.010
60	4000	1.155
65	4300	1.263
70	4600	1.371
75	5000	1.516
80	5300	1.696
85	5600	1.913
90	6000	2.129
95	6300	2.238
100	6600	2.526
105	7000	2.779
110	7300	3.031

TABLE A-7 (cont'd)

GPM	RE	ΔP_{SI}
115	7600	3.212
120	8000	3.428
125	8300	3.681
130	8600	3.970
135	9000	4.258
140	9300	4,583
145	9600	4,728
150	10000	5.052
155	10300	5.485
160	10600	5.918
165	11000	5.991

TABLE A-8

SUBCHANNEL PRESSURE DROP DATA FOR THE FOUR INCH LEAD BUNDLE (EDGE SUBCHANNEL)

GPM	RE	P_{SE}
30	2000	0.397
35	2300	.496
40	2600	.541
45	3000	.722
50	3300	.866
55	3600	1.010
60	4000	1.191
65	4300	1.299
70	4600	1.407
75	5000	1.552
80	5300	1.660
85	5600	1.840
90	6000	2.093
95	6300	2.201
100	6600	2.346
105	7000	2.670
110	7300	2.851

TABLE A-8 (cont'd)

GPM	RE	ΔP_{SE}
115	7600	3.068
120	8000	3.320
125	8300	3.537
130	8600	3.825
135	9000	4.078
140	9300	4.258
145	9600	4.403
150	10000	4.764
155	10300	5.088
160	10600	5.413
165	11000	5.738

APPENDIX B

Error Analysis

The error involved in the determination of the friction factor is composed of two parts: the experimental error in the subchannel pressure drop measurement and in the subchannel flow rate measurement, and the data reduction error. The data reduction error is mainly due to the simplification made in Eq. (4-2) to determine the bundle average pressure drop. Section (B-1) evaluates the maximum expected error involved in the subchannel pressure drop measurement and Sect. (B-2) evaluates the data reduction error. Section (B-3) relates these two errors and the experimental error involved in the determination of the average subchannel flow rate, to the errors involved in the determination of the bundle average friction factors and the local subchannel friction factors.

B-1 Experimental Error in Subchannel Pressure Drop Measurement

The experimental error is usually comprised of two types of errors: random error and systematic error. In this experiment, the random error results from the following factors:

1) fluctuation of the loop flow rate

2) misjudgement of the reading on the static pressure gauge

3) fluctuation of the subchannel local static pressure.

The systematic error is mainly due to the deficiency of the static pressure gauge. In what follows, we will evaluate all the errors corresponding to the aforementioned causes.

In the evaluation of the random error, the component due to the fluctuation of the subchannel local static pressure can be omitted because of its high frequency nature (usually about 10 to 100 hz). The strain gauge used in this experiment does not respond to this high frequency fluctuation and in fact gives a very stable reading corresponding to the mean value of the subchannel static pressure. The fluctuation of the loop flow rate is not high frequency in nature. It usually takes about five seconds to go through a fluctuation cycle. This may cause errors in the determination of the static pressure from the strain gauge. The maximum expected error in the loop flow due to this fluctuation is estimated to be 3% by visually observing the fluctuation in the float of the loop flow rotameter. This error in turn may cause an error in the determination of the subchannel static pressure of about 5% $(1.03)^2$ since the static pressure is proportional to the square of the velocity.

The random error involved in the reading of the static pressure gauge is about ± 0.1 inch of water. Therefore, this leads to about $\pm 15\%$ error in the determination of the static pressure drop at the bundle Reynolds number of 200. However, this error will decrease as the bundle flow rate increases since the static pressure drop increases as the bundle flow rate increases, and since this error is determined by the ratio of the observation error to the total subchannel pres-

sure drop. For example, at a Reynolds number of 500, this error can only cause ±7.5% uncertainty in the determination of the pressure drop, and at bundle Reynolds number 1000, this error will induce only ±3% uncertainty in the determination of the subchannel pressure drop. For reasons of conservatism, a 3% error is imposed on the static pressure drop determination for a bundle Reynolds number larger than 1000.

The systematic error due to the accuracy of the pressure gauge is estimated to be ±1%. The gauges were calibrated to this accuracy by the manufacturer before this experiment was performed.

From the above discussion, we can evaluated the total experimental error as the sum of the total random error from the statistical combination of the loop flow fluctuation and the experimenter's misjudgement in reading the static pressure gauge plus the systematic error due to accuracy of the pressure gauge. Thus, the total errors are:

$$\text{Experimental total error} = \pm\left(\sqrt{0.06^2 + 0.03^2} + 0.01\right)$$
$$= \pm 7.7\% \text{ for } Re > 1000 \qquad \text{(B-1)}$$

and

$$\text{Experimental total error} = \pm\left(\sqrt{0.06^2 + 0.075^2} + 0.01\right)$$
$$= \pm 9.6\% \text{ at } Re = 500 \qquad \text{(B-2)}$$

and

$$\text{Experimental total error} = \pm\left(\sqrt{0.06^2 + 0.15^2} + 0.01\right)$$
$$\pm 17.2\% \text{ at } Re = 200 \qquad \text{(B-3)}$$

B-2 Error in Data Reduction

The simplification made in Eq. (4-2) to determine the bundle average pressure is based on the assumption that the pressure drops for all the interior subchannels over a certain subchannel length are the same and that the pressure drop for all the edge subchannels over a certain subchannel length are also the same. This assumption is deduced from the experimental fact that the subchannel flow rates for all the interior subchannels are not affected by the existence of the edge subchannels even for those interior subchannels located near the edge subchannels (Ref. 4). This feature implies that the hydraulic characteristics of the interior subchannels depend only on their own geometric parameters. Since the geometric characteristics for all the interior subchannels are the same, it is expected that the interior subchannel pressure drops will be the same over a certain subchannel length.

However, if the above deduction is wrong, i.e., if the interior subchannel pressure drop is not the same for every interior subchannel, an error will result from the use of Eq.(4-2) in the determination of P_b. For the sake of conservatism, we assume that the pressure drop of the average interior channel is midway between that of our measured center interior channel and edge channel, i.e.:

$$\overline{P_{s1}} = (P_{s1} + P_{s2}) / 2.0 \qquad \text{(B-4)}$$

where P_{sI} is the subchannel pressure drop for the center interior subchannel.

Thus, the total data reduction error in P_b becomes

$$\text{Data Reduction Error} = \frac{\dfrac{\Delta P_{s1} A_{s1} N_1 + \Delta P_{s2} A_{s2} N_2}{N_1 A_{s1} + N_2 A_{s2}} - \dfrac{\overline{\Delta P_s} A_{s1} N_1 + \Delta P_{s2} A_{s2} N_2}{N_1 A_{s1} + N_2 A_{s2}}}{\Delta P_b} \tag{B-5}$$

Inserting Eq. (B-4) into the above equation, we obtain:

$$\text{Data Reduction Error} = \frac{0.5(\Delta P_{s1} - \Delta P_{s2})}{0.5\ \Delta P_{s1} + \Delta P_{s2}(A_{s2} N_2 / A_{s1} N_1 + 0.5)} \tag{B-6}$$

In this experiment, $(A_{s2} N_2 / A_{s1} N_1) = 0.545$, therefore Eq. (B-6) becomes:

$$\text{Data Reduction Error} = \frac{0.5(\Delta P_{s1} - \Delta P_{s2})}{0.5\ \Delta P_{s1} + 1.045\ \Delta P_{s2}} \tag{B-7}$$

Inserting the experimental data of ΔP_{s1} and ΔP_{s2} into the above equation, we find the maximum data reduction error in ΔP_b to be equal to 3.8% which corresponds to a bundle flow of 165GPM in the four inch lead bundle.

B-3 Total Error in the Determination of the Friction Factors

From the following relationship between friction factors and the pressure drop:

$$\Delta P = f \frac{L}{De} \frac{\rho V^2}{2 g_c}, \tag{B-8}$$

we can relate the error in the determination of ΔP and V to the error in the friction factor by changing the above equation into its differential form, i.e.,

$$\delta(\Delta P) = \frac{L}{De} \frac{\rho V^2}{2g_c} \delta f + f \frac{LV}{De} (\delta V). \qquad \text{(B-9)}$$

Rearranging the above equation, we obtain

$$(\frac{\delta f}{f}) = \frac{\delta \Delta P}{\Delta P} + 2(\frac{\delta V}{V}) \qquad \text{(B-10)}$$

where $\frac{\delta f}{f}$ = relative error in the determination of the friction factor

$\frac{\delta \Delta P}{\Delta P}$ = relative error in the determination of the pressure drop

$\frac{\delta V}{V}$ = relative error in hte determination of the velocity

The Eq.(B-10) is a general equation to determine the relative error in the determination of the friction factor. Therefore, to determine the error in the bundle average friction factor, the errors in the determination of the bundle average pressure drop and the bundle average velocity should be taken into account. For the error in the subchannel friction factor, the errors in the determination of the subchannel pressure drop and the subchannel average velocity should be taken into account. Section (B-3-1) evaluates the error involved in the determination of the bundle average friction factor and Sect. (B-3-2) evaluates the error involved in the

determination of the local subchannel friction factors for both interior and edge subchannels.

B-3-1 Error in Bundle Average Friction Factors

The error in the bundle average friction factor is induced by the errors involved in the determinations of ΔP_b and of the bundle average velocity. The error in ΔP_b is comprised of two components: the data reduction error and the subchannel pressure drop measurement error. Thus, the error involved in the determination of ΔP_b is equal to

$$\frac{\delta \Delta P_b}{\Delta P_b} = \text{data reduction error} + \text{measurement error}$$

$$= \begin{cases} 11.5\% & \text{for Re} > 1000 \\ 13.4\% & \text{at Re} = 500 \\ 21.0\% & \text{at Re} = 200 \ . \end{cases} \qquad \text{(B-11)}$$

At the same time, we know that $\frac{\delta V}{V}$ is equal to the error in the determination of the loop flow, evaluated in Sect. (B-1) to be ±3%. Therefore, the error inherent in the bundle average friction factor can be evaluated from Eq. (B-11). The results are stated as follows:

$$\frac{\delta f}{f} = \begin{cases} 17.5\% & \text{for Re} > 1000 \\ 19.4\% & \text{at Re} = 500 \\ 27.0\% & \text{at Re} = 200 \ . \end{cases} \qquad \text{(B-12)}$$

B-3-1 Error in Local Subchannel Friction Factor

The error involved in the determination of the local subchannel friction factor is induced from the errors involved in the determinations of the subchannel pressure drop and of the subchannel average velocities. In Ref. (4), the error of $\frac{\delta V}{V}$ is evaluated to be ±5%. The error of the subchannel pressure measurement, i.e., $\frac{\delta \Delta P_s}{\Delta P_s}$, is estimated in Sect. (B-1) to be

$$\frac{\delta \Delta P_s}{\Delta P_s} = \begin{cases} \pm\ 7.7\% & \text{for Re} > 1000 \\ \pm\ 9.6\% & \text{at Re} = 500 \\ \pm 17.2\% & \text{at Re} = 200\ . \end{cases} \qquad \text{(B-13)}$$

From Eq. (B-10) and the above information, the relative error in the local subchannel error is evaluated as:

$$\frac{\delta f}{f} = \begin{cases} \pm 17.7\% & \text{for Re} \quad 1000 \\ \pm 19.6\% & \text{at Re} = 500 \\ \pm 27.2\% & \text{at Re} = 200\ . \end{cases} \qquad \text{(B-14)}$$

REFERENCES

[1] C. Chiu, N.E. Todreas and W.M Rohsenow, "Mixing Experiment in LMFBR Blanket Assemblies," to be issued as a topic report COO-2245-39TR, Department of Nuclear Engineering, M.I.I., 1977.

[2] K. Rehme, "Pressure Drop Correlations for Fuel Element Spacers," Nuclear Technology, Vol. 17, (15-21), January 1973.

[3] E.H. Novendstern, "Turbulent Flow Pressure Drop Model for Full Rod Assemblies Utilizing a Helical Wire-wrap Spacer System," Nuclear Engineering and Design, 22-1, August, 197 .

[4] C. Chiu, N.E. Todreas and W.M. Rohsenow, "Flow Split Measurements in LMFBR Blanket Assemblies," to be issued as a topic report COO-2245-45TR, Nuclear Engineering Department, M.I.T., 1977.

[5] C. Chiu, W.M. Rohsenow and N.E. Todreas, "Flow Split Model for LMFBR Wire Wrapped Assemblies", COO-2245-56TR, Department of Nuclear Engineering, M.I.T. December, 1977.